The influence of cross-linking density on the efficiency of post-synthetic sulfonation of hyper-cross-linked polymers and their adsorption capacity for antibiotic pollutants

Joanna Wolska[a,*], Malwina Muńko[b], Hussein EL Siblani[c], Igor Telegeiev[c], Marcin Frankowski[a], Anna Szwajca[a], Justyna Walkowiak-Kulikowska[a], Mohamad El-Roz[c], Lukasz Wolski[a]

[a] *Faculty of Chemistry, Adam Mickiewicz University, Poznań, ul. Uniwersytetu Poznańskiego 8, 61-614 Poznań, Poland*

[b] *Center for Advanced Technology, Adam Mickiewicz University, ul. Uniwersytetu Poznańskiego 10, 61-614 Poznań, Poland*

[c] *Laboratoire Catalyse et Spectrochimie, Normandie Université, ENSICAEN, UNICAEN, CNRS, Caen, 14050, France*

** Corresponding author: j.wolska@amu.edu.pl (J. Wolska)*

Abstract:

Hyper-cross-linked polymers (HCPs) attract increasing attention as promising adsorbents for removal of organic pollutants from water. The present work reveals for the first time that the efficiency of the post-synthetic sulfonation of HCPs-based adsorbents and their reactivity in removal of selected polar antibiotic pollutants can be simply controlled by adjusting the cross-linking density of the polymer network. The study included both the evaluation of the mechanism and kinetics of the adsorption process over sulfonated HCPs, as well as the determination of their stability, recyclability, and affinity toward various antibiotics. The latter was established based on adsorption tests using mono- and multicomponent mixtures of different structure antibiotics (ciprofloxacin, tetracycline, sulfamethoxazole and amoxicillin). The adsorption capacity of all sulfonated polymers was found to be directly proportional to the concentration of $-SO_3H$ functions and inversely proportional to the cross-linking density of the parent HCPs. The most promising sulfonated polymer had approximately 4 times higher adsorption capacity toward ciprofloxacin than commercial carbon-based adsorbent *Norit* (427.5 vs. 110.5 mg/g, respectively). The main adsorption mechanism over sulfonated HCPs was chemisorption of the antibiotics via ionic interactions with surface $-SO_3H$ groups. Spent adsorbent could be successfully recycled ten times without any loss in its efficiency.

Keywords:

hyper-cross-linked polymers; sulfonic acid functionalization; water purification; antibiotic.

1. Introduction

Undeniably, the wide spread of antibiotics in human medicine can be considered as breakthrough point in the history that has allowed for tremendous success in improving health outcomes for all of humanity [1]. However, despite of its undisputable advantages, the growing production and consumption of these pharmaceuticals has also a dark side as approximately 30–90% of the initial antibiotic dose ingest for a specific therapeutic treatment is not absorbed and discharged into the environment, mainly through municipal sewage [2–4]. This situation is of great concern, as even sublethal concentration of the antibiotic residues in natural environment can generate antimicrobial resistance of living bacteria [5]. To avoid the above-mentioned issue, it is extremely urgent to develop new and highly effective methods of eliminating antibiotic residues from wastewater [6,7]. Among various methods of wastewater remediation, adsorption-based technologies are currently receiving particular attention, coming to the forefront due to their cost-effectiveness, facile operating conditions, and ease of scale-up [8]. To date, majority of fundamental research in this field has focused on understanding and improving the reactivity of nanomaterials based on activated carbon [9] or mineral clay [10], which are still considered among the most promising and efficient adsorbents. Recently, however, increasing attention is directed to the development of a relatively new class of adsorbents based on metal-organic frameworks (MOFs) [11–13] and porous organic polymers (POPs) [14,15], that exhibit a number of unique properties and significantly outperform other previously used materials in terms of cost, adsorption capacity, stability, recyclability and versatility.

Hyper-cross-linked polymers (HCPs) belong to the POPs family and are characterized by high surface areas (more than 1000 m^2/g), tunable porosities, as well as high mechanical, chemical, and hydrothermal stabilities [16]. Despite the aforementioned highly desirable properties of HCPs as potential adsorbents, the great interest in the application of these

nanomaterials for wastewater remediation is also due to the availability of their cost-effective large-scale production by relatively easy, inexpensive and scalable method based on Friedel-Crafts alkylation (one-step knitting procedure reported by Tan et al. [17]). To date, HCPs-based nanomaterials have been applied mainly in the separation of gases like CO_2 [18–21] or CH_4 [22–25]. However, a recent review article [26] clearly indicates that these materials may also be promising candidates for adsorptive removal of various aqueous contaminants, like toxic metals or hazardous organic dyes.

Concerning recent achievements in the development of novel HCPs-based adsorbents for gas phase separation processes, it was documented that the specific surface area, porosity and adsorption capacity of these nanomaterials are strongly affected by the cross-linking density (the molar ratio between the aromatic building block and the cross-linker) [27–30]. Interestingly, all of these structure-induced features of HCPs mentioned above were found to be strongly related not only to the type of cross-linker itself, but also to the character of the aromatic building block. For HCPs-based adsorbents obtained by knitting method using a relatively small building blocks such as benzene, the highest adsorption capacities toward CO_2 [29] or ethane [30] were observed for the materials prepared with relatively low amount of the alkylating cross-linker (benzene to the cross-linker molar ratio of 1.0:3.0 [29] or even 1.0:1.5 [30]). The relationship was, however, totally different when larger and rigid aromatic building blocks were used in the synthesis of HCPs-based adsorbents. Two independent research groups proved that the highest adsorption capacity against CO_2 [31] and toluene vapors [27] was achieved for the tetraphenylmethane-based adsorbents with a fair excess of cross-linker during their synthesis with a molar ratio of the aromatic building block to the cross-linker equal to 1.0:16.0. However, to the best of our knowledge, the influence of the cross-linking density of HCPs on their adsorption capacity in the removal of large polar organic pollutants from liquid phase, where the porosity of a polymer may have a more pronounced impact on the diffusion

of these model pollutants in the polymer network than observed in previous studies for smaller molecules in a gas phase has not yet been investigated.

As concerns adsorptive removal of water-soluble and polar organic pollutants from aqueous solutions, it was documented that the adsorption capacity of HCPs-based nanomaterials is strongly dependent on their surface properties, and can be significantly enhanced by increasing the polarity of the polymer network through post-synthetic sulfonation. Giri et al. [15], for instance, reported that adsorption capacity of triptycene-based HCPs to methylene blue dye was increased 2.2-fold (from a removal efficiency of 30 to 66%) when sulfonic acid species were introduced to the polymer surface. This strongly enhanced reactivity of HCPs after the post-synthetic modification was due to the fact that methylene blue was adsorbed mainly through ionic interactions with $–SO_3H$ functional groups, rather than π-π stacking with an aromatic polymer matrix. However, the study by Giri et al. [15] did not evaluate the effect of HCPs cross-linking density on the physicochemical properties of these polymers (e.g., surface area, porosity, etc.), as well as the efficiency of sulfonic acid species incorporation into the polymer network via the post-synthetic sulfonation. It is highly probable that both of these parameters can have decisive impact on the nature of interaction between various polar organic pollutants and the polymer surface, and thus on the adsorption capacity of HCPs-based sulfonated nanomaterials.

The present study aimed at unraveling the effect of the cross-linking density of hyper-cross-linked polymers based on triphenylmethane (TPM) as aromatic building block and formaldehyde dimethyl acetal (FDA) as a cross-linking agent on the efficiency of their post-synthetic sulfonation. Of particular interest was the evaluation of the influence of the physicochemical properties of the parent HCPs-based materials, characterized by different cross-linking density, on the efficiency of sulfonic acid species incorporation into the polymer network as well as on the stability, recyclability, and adsorption capacity of the resulting

sulfonated materials in the removal of selected antibiotics commonly used in human medicine (ciprofloxacin, tetracycline, sulfamethoxazole and amoxicillin). A significant part of this work also covered a detailed analysis of the mechanism and kinetics of the adsorption process over sulfonated HCPs (sHCPs), as well as gaining insight into the versatility of the prepared polymers in the removal of antibiotics of different type and structure both from single-component and ternary mixtures.

2. Experimental Methods

2.1. Chemicals and reagents

Chemicals and reagents used in this study were the following: triphenylmethane (TPM, Sigma-Aldrich, 99%), formaldehyde dimethyl acetal (FDA, Sigma-Aldrich, 99%), ferric chloride ($FeCl_3$, Sigma-Aldrich, anhydrous for synthesis), 1,2-dichloroethane (DCE, Sigma-Aldrich, anhydrous, 99.8%), chlorosulfonic acid ($ClSO_3H$, Sigma-Aldrich, 99%), methanol (CHEMSOLUTE, 99.8%), acetonitrile (Merck KGaA, hypergrade for LC-MS), water (Merck KGaA, LC-MS grade), formic acid (VWR, ≥ 99%, LC-MS grade), nitric acid (HNO_3, Chempur, 65%), sodium hydroxide (NaOH, POCH, reagent grade), ciprofloxacin (CIP, Sigma-Aldrich, ≥ 98%, HPLC grade), tetracycline (TC, Sigma-Aldrich, 98.0-102.0%, HPLC grade), sulfamethoxazole (SMX, Sigma-Aldrich, analytical standard), amoxycillin (AMX, Sigma-Aldrich, 95.0-102.0% anhydrous basis). The commercial activated carbon (*Norit* SX 2, Chempur) and hydrogen form of Amberlyst-15 (Sigma-Aldrich) were used as reference materials for the research and labelled as *Norit* and *Amberlyst-15*, respectively. All chemical were used as received. Deionized water was used throughout the experiments.

2.2. Preparation of HCPs

All pristine HCPs polymers were prepared by Friedel-Crafts alkylation [17] using triphenylmethane (TPM) and formaldehyde dimethyl acetal (FDA), as a commercially available building block and cross-linker, respectively. In a typical synthesis procedure, TPM (2.44 g, 10

mmol, 1 equiv.) and $FeCl_3$ (45 mmol, 4.5 equiv.) were dispersed in DCE (60 mL) under an argon atmosphere. Following 15 min of vigorous stirring at room temperature, FDA (3.42 mL, 45 mmol, 4.5 equiv.) was added dropwise to the above suspension resulting in formation of brown thick gel. The obtained gel was stirred at 40 °C for 5 h, then heated to 80 °C and stirred for another 24 h. During the heating step, the polymer precipitated out of the solution as a brown solid. After cooling to room temperature, the precipitate was separated through Büchner filtration, washed with methanol until a colorless filtrate was obtained, and then with water. The resulting brown product (HCP1) was Soxhlet extracted with methanol for 72 h and then dried under vacuum at 80 °C to constant mass (Yield: 3.0 g, 98%). HCP2 (Yield: 3.6 g, 96%) and HCP3 (Yield: 4.1 g, 95%) polymers were prepared according to the same experimental procedure, but using different TPM to FDA molar ratio (1.0:9.0 and 1.0:13.5 for HCP2 and HCP3, respectively).

The % yield of HCPs was calculated using following equation (Eq. 1):

$$\%\ yield = \frac{m_{HCP}}{m_{TPM} + m_{methylene\ linker}} \qquad \text{(Eq. 1)}$$

where m_{HCP}, m_{TPM} and $m_{methylene\ linker}$ are the mass of the respective HCP (after Soxhlet purification and drying), triphenylmethane used for polymerization and $-CH_2-$ moiety (derived from FDA) incorporated into the polymer network, respectively.

2.3. Preparation of sulfonated HCPs

Sulfonated HCPs were prepared by a facile post-synthetic sulfonation procedure [32]. For this purpose, the pristine HCP (1.5 g) was stirred into DCE (50 mL) and agitated at room temperature for 1 h to allow the polymer network to swell in the solvent. The resulting suspension was cooled to 0 °C, and then chlorosulfonic acid (10 mL) was added dropwise under vigorous agitation. Following 72 h of intensive stirring at room temperature, the above mixture was poured into 500 mL of deionized water and stirred for 1 h to quench unreacted chlorosulfonic acid. Finally, the sulfonated polymer was separated by Büchner filtration and

washed thoroughly with water and methanol until the pH of filtrate was neutral (no acid residual in the filtrate). The as-prepared dark brown solid was dried under vacuum at 80 °C to constant mass. The yields were 1.9 g, 1.7 g and 1.6 g for sHCP1, sHCP2 and sHCP3, respectively.

2.4. Characterization of materials

Solid-state proton-decoupled ^{13}C CP/MAS NMR experiments were performed on a Bruker AV III 500MHz spectrometer operating at a Larmor frequency of 125.7 MHz for ^{13}C. Spectra were obtained using a Bruker 4 mm double resonance MAS probe with sample spinning rate at 12 kHz, 8192 transients were added with a recycling delay of 3 s and a contact time of 1000 ms was employed. The ^{13}C chemical shifts were referenced to TMS.

The FTIR spectra of the polymers were acquired in the range of 4000 cm^{-1} to 400 cm^{-1} (resolution 4 cm^{-1}, number of scans = 64) using a Vertex 70 spectrometer (Bruker). For FTIR measurements with KBr, the samples were dispersed in KBr pellet (2 mg of the sample and 200 mg of KBr).

The wettability properties of the catalyst materials were evaluated by water contact angle (CA) measurements at room temperature and relative humidity of 12% (DataPhysics Instruments GmbH, OCA 15). It was observed by placing a drop of water on the polymer surface and measuring the angle using the sessile drop type. A camera captured images of the droplets as quickly as possible after their deposition. The droplet after contact with the surface was analyzed to obtain the contact angle values with an accuracy of 0.1 degrees (°).

X-ray photoelectron spectroscopy (XPS) was performed using an ultra-high vacuum photoelectron spectrometer based on a Phoibos150 NAP analyzer (Specs, Germany). The analysis chamber was operated under vacuum with a pressure close to 5×10^{-9} mbar and the sample was irradiated with a monochromatic AlKα (1486.6 eV) radiation. Any charging that might occur during the measurements (due to incomplete neutralization of ejected surface

electrons) was accounted for by rigidly shifting the entire spectrum by a distance needed to set the binding energy of the C 1s assigned to adventitious carbon to the assumed value of 284.8 eV.

Elemental analysis (EA) of the HCPs was carried out with an Elementar Analyser Vario EL III. The samples were weighed in tin capsules (4 mg) and introduced into the reactor with a precisely defined portion of oxygen. After combustion at 900-1000 °C, the exhaust gases were transported in helium flow to the second reactor, and then through the water trap to the chromatographic column, which separated the generated gases. Finally, the separated gases were detected by a thermal conduction detector (TCD). The measurements were repeated three times for each investigated sample.

The sulfonic acid ($-SO_3H$) exchange capacity of all HCPs were determined by acid-base titration method using NaCl aqueous solution as an ion-exchange agent [33]. In a typical procedure, 0.100 g of dry polymer (drying conditions: 80 °C for 12 h under vacuum) was immersed in a 2.0 M NaCl aqueous solution (60 mL) and stirred at room temperature for 48 h. Then, the resulting suspension was filtrated off and the filtrate was titrated with 0.005 M NaOH aqueous solution using phenolphthalein as an indicator. The acid exchange capacity in the polymer was calculated using the following equation (Eq. 2):

$$acid\ exchange\ capacity = C_{NaOH} \times \Delta V/m \qquad \text{(Eq. 2)}$$

where C_{NaOH} represents the concentration of the NaOH solution, m is an initial mass of polymer and ΔV is the volume of the NaOH solution consumed during acid-base titration method.

Scanning electron microscopy (SEM) images were recorded using a Quanta 250 FEG, FEI instrument. Samples were mounted on carbon tape on aluminum stubs, without any coating treatment.

N_2 adsorption-desorption isotherms were obtained at –196 °C using an Autosorb iQ Analyzer (Quantachrome). Before measurements, the samples were degassed at 80 °C for 22 h. The specific surface area of the materials obtained was calculated by the Brunauer-Emmett-

Teller (BET) method, and the average pore size was estimated by the Barrett-Joyner-Halenda (BJH) method from the desorption branch of the isotherm.

Thermogravimetric analysis (TGA) experiments of polymers were performed with a STA 6000 apparatus from Perkin Elmer, under a nitrogen atmosphere, at the heating rate of 10 °C/min from room temperature up to a maximum of 900 °C.

Measurements of the zeta potential as a function of the pH of the aqueous dispersion of the polymer samples were performed on Zetasizer Nano ZS (Malvern). The zeta potential was estimated from electrophoretic mobility by using the Henry equation: $U_{\mathrm{E}} = 2\varepsilon\zeta F(\mathrm{ka})/3\eta$, where U_{E} is the electrophoretic mobility, ζ the zeta potential, ε the dielectric constant, $F(\mathrm{ka})$ Henry's function (set for 1.5 as in the Smoluchowski approximation), and η the viscosity. The pH value was adjusted with 0.1 mol/L of HCl or NaOH solutions.

2.5. Adsorption experiments

All adsorption tests were performed in a bath reactor (250 mL). In a typical experiment, 5 mg of the polymer (adsorbent loading = 0.025 g/L) was added to 200 mL of aqueous solution of an antibiotic (C_0 = 15 mg/L) under vigorous stirring (600 rpm). After a given adsorption time (t), the efficiency of the antibiotic removal was estimated on the basis of UV-vis measurements. For this purpose, 4 mL aliquots were collected into a syringe and the adsorbent was separated from the solution by filtration through a 0.2 μm syringe filter (PTFE, Lab Logistics). The syringe filter was conditioned by washing with a small portion of the previously collected solution, and no noticeable adsorption of the antibiotic on the filter was observed. The adsorption spectrum of the filtrate was recorded by using a spectrophotometer (Varian Cary 300) in the range 200-400 nm with water as a reference. The antibiotic removal efficiency was calculated using the following equation (Eq. 3):

$$antibiotic\ removal\ efficiency\ (\%) = \frac{(C_0 - C_t)}{C_0} \times 100 \qquad \text{(Eq. 3)}$$

where C_0 and C_t are the initial and final (after time, t, of the adsorption) concentration of the antibiotic, respectively. In whole CIP concentration range used in this study, a linear correlation was observed between absorbance (λ_{max} = 271 nm) and concentration of the antibiotic (Fig. S1). All adsorption experiments were performed at least two times. The experimental error related to the determination of antibiotic removal efficiency was lower than 5% of the measured value. Adsorption tests with the use of real environmental matrices (tap water: Morasko, Poznań, Poland, and river water: Warta River, sample collected in Biedrusko, Poland) were performed under the same experimental conditions. Before the measurements, solid particles from water samples were separated by filtration. Then, given amount of CIP was dissolved in the filtrate. As-prepared aqueous solution of the antibiotic was subjected to adsorption tests. Efficiency of CIP removal was determined by means of UV-vis spectroscopy using given water sample (filtrated river or tap water) as reference.

The kinetics of adsorption was analyzed based on pseudo-first-order and pseudo-second-order linear models [34] as well as the intraparticle diffusion (ID) model [35,36]. More details are provided in the extended experimental section (see Supplementary Data, SD). During experiments under acidic or alkaline conditions, the pH of the antibiotic solution was adjusted before the addition of adsorbents with the use of diluted nitric acid or sodium hydroxide. To exclude possible diffusion limitation effects during the adsorption tests, series of experiments at different stirring rates were performed (Figs. S2 and S3). Increasing a stirring rate from 400 to 600 rpm resulted in noticeable increase in the efficiency of CIP removal. However, further increase of stirring rate to 700 rpm had no significant influence on CIP removal efficiency. Therefore, a stirring rate of 600 rpm was chosen for all adsorption experiments.

Isotherms of the ciprofloxacin adsorption were recorded in bath mode using Easy-Max (Mettler-Toledo) work station equipped with thermocouple to control the reaction temperature. Experimental data were fitted to Langmuir and Freundlich adsorption models. Details related

to calculations and treatment of data are described in extended experimental section (SD). Gibb's free energy (ΔG^0), was determined according to Eq. (4).

$$\Delta G = -RT \ln(K_L) \quad \text{Eq. (4)}$$

where, T is the solution temperature (K, 20°C), R is the ideal gas constant (8.314 J mol^{-1} K^{-1}) and K_L is the adsorption capacity constant (L/g) derived from Langmuir isotherm model. Since K_L should be unitless to get the correct units, the Langmuir isotherm coefficient K_L was converted into a dimensionless constant by multiplying it by 1000 [37].

Infrared spectra of sHCP1 polymer after CIP adsorption were acquired by using a Bruker Vertex 70 spectrophotometer equipped with an attenuated total reflectance (ATR) accessory (Bruker). Before ATR-IR measurements, the samples after adsorption tests were separated from aqueous solutions of antibiotic by filtration and dried under vacuum at 60 °C for 24 h. The same sample was also subjected to XPS analysis under conditions described above (please see Section 2.4).

The LC–MS/MS system included a Shimadzu Liquid Chromatography system coupled to a Shimadzu 8050 triple quadrupole mass spectrometer (Shimadzu, Japan). The UHPLC system consisted of a solvent delivery system (two pumps Nexera X2 LC-30AD), an autosampler (Nexera X2 SIL-30AC), degasser (DGU-20A5R), a column oven (CTO-20AC) and a system controller (CBM-20A). Compounds were chromatographically separated on a Kinetex C18 (2.1 × 100 mm, 2.6 um) column with isocratic elution using (A) water (0.1% formic acid) and (B) acetonitrile (0.1% formic acid) as mobile phases A and B (60%/40%), respectively. The flow rate was 0.4 mL/min, and the total run time was 5.0 min. Operating conditions of the mass spectrometer were as follows: Ionization: ESI positive; DL temp.: 250 °C; Interface temp.: 300 °C; Block heater temp.: 500 °C; Nebulizer gas flow: 3 L/min; Drying gas flow: 10 L/min; Heating gas flow: 10 L/min; Dwell time: 20 ms; Pause time: 1 ms. Optimized MRM transitions for each analyte were as follows: ciprofloxacin (331.8-314.0;

331.8-231.0), tetracycline (444.8-410.1; 444.8-427.1) and sulfamethoxazole (253.9-156.0; 253.9-108.1). Standards solutions were prepared from ciprofloxacin, tetracycline and sulfamethoxazole with the concentration of 1000 mg/L in methanol (Merck, Poland) for LC-MS/MS.

2.6. Reuse tests and regeneration procedure

In typical reuse experiment, 20 mg of sHCP1 (adsorbent loading = 0.100 g/L) was added to 200 mL of CIP solution (C_0 = 15 mg/L) under vigorous stirring (600 rpm). Following 45 min of agitation at room temperature (adsorption step), the sHCP1 was separated from the solution through PTFE filter paper (Biosens, 0.22 μm) on a glass vacuum filtration apparatus (Whatman). Concentration of the antibiotic in the filtrate was analyzed on the basis of UV-vis measurements, and the efficiency of antibiotic removal after a given adsorption cycle was determined using equation (Eq. 3). To regenerate of the spent adsorbent, the polymer separated after the adsorption step was dispersed in 50 mL of 1.0 M HCl solution and agitated for 60 min at room temperature (stirring rate = 300 rpm). The regenerated adsorbent was then washed thoroughly with deionized water until neutral pH and subjected directly to the next adsorption cycle. The regeneration performance of sHCP1 was studied in a total of ten adsorption-desorption cycles. For comparison purposes, several reuse tests were performed with the use of ethanol instead of 1.0 M HCl solution. This allowed further elucidation of the nature of interaction between adsorbent and adsorbate (chemisorption vs. physisorption) [38].

3. Results and discussion

3.1. Adsorbents preparation and characterization

A series of hyper-cross-linked polymers (HCP1, HCP2 and HCP3) were knitted based on Friedel-Crafts alkylation [17] using triphenylmethane (TPM) and formaldehyde dimethyl acetal (FDA), as a commercially available aromatic building block and alkylating cross-linker, respectively. During the reaction, TPM was cross-linked via the methylene bridges (−CH_2−) of

FDA and polymerized into a hyper-cross-linked porous polymer material (Scheme 1A). First, the reaction was carried out with a TPM:FDA molar ratio of 1.0:4.5, which is lower than the ratio required for full cross-linking polymerization. The resulting material was labeled as HCP1. Subsequently, HCP2 material with an over-stoichiometric TPM:FDA molar ratio of 1.0:9.0 was prepared. Finally, "forced" cross-linking conditions were also explored by synthesizing a polymer HCP3 with a TPM:FDA ratio of 1.0:13.5. In the next steps, the as-prepared pristine HCPs were functionalized by post-synthetic sulfonation using chlorosulfonic acid as the sulfonating agent, yielding the corresponding sulfonated HCPs (labeled as sHCP1, sHCP2 and sHCP3; Scheme 1B).

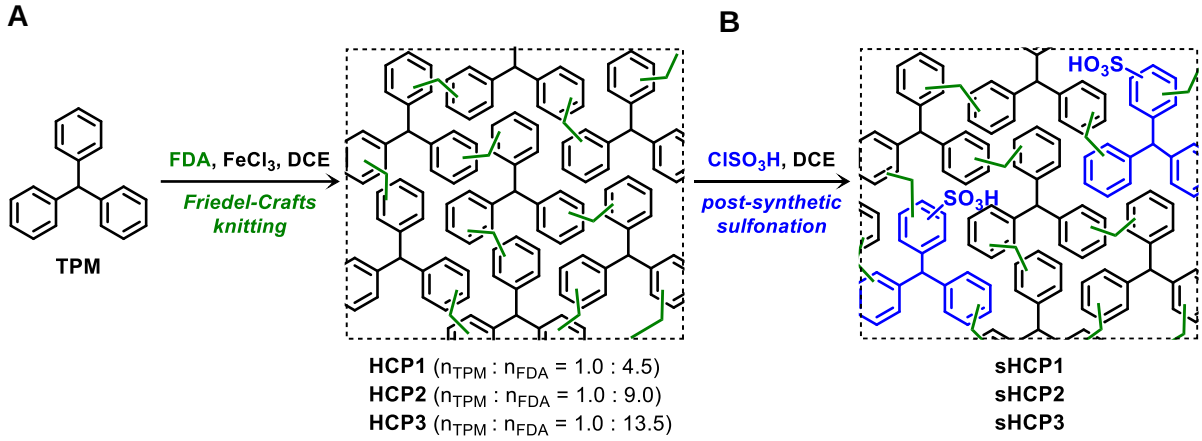

Scheme 1. The two-step synthetic pathway for the preparation of sulfonated triphenylmethane-based hyper-cross-linked polymers (sHCP1-sHCP3) by (A) the Friedel-Crafts alkylation using an formaldehyde dimethyl acetal (FDA) as an external cross-linker and (B) the post-synthetic sulfonation of the parent HCP polymers using chlorosulfonic acid ($ClSO_3H$) as a sulfonating agent. DCE stands for 1,2-dichloroethane.

The successful cross-linking of triphenylmethane-based HCP with formaldehyde dimethyl acetal was confirmed by the solid state CP/MAS ^{13}C NMR spectroscopy. As shown in Fig. 1A, the CP/MAS ^{13}C NMR spectra of all HCPs revealed the presence of broad peaks in the range of 110−145 ppm (region a) and a peak at approximately 48 ppm (region b)

corresponding to aromatic carbons [15,39] and sp^3-hybridized tertiary carbon species of TPM [40], respectively. Moreover, the presence of peaks in the range of 20−37 ppm (region c) confirmed successful polymerization of TPM through cross-linker-derived methylene bridges [15]. Comparison of the CP/MAS ^{13}C NMR spectra of the pristine HCPs and their sulfonated counterparts (Fig. 1A) showed no significant differences. This implied that post-synthetic sulfonation had no adversely effects on the structure of the pristine polymers.

The chemical structure of all prepared hyper-cross-linked porous materials was also investigated by FTIR spectroscopy. As can be seen in Figs. 1B and S4, IR bands typical of stretching vibrations of sp^2-hybridized C−H and C=C bonds of TPM core are observed for all polymers in the range from 3100 to 3000 cm^{-1} [15] (region b), and 1600 to 1450 cm^{-1} [41] (region d), respectively. In all IR spectra, one can also observe bands characteristic of the cross-linking methylene bridges which are overlapped with the stretching vibrations of the C−H bonds of sp^3-hybrized carbon of TPM core (bands in the range from 2930 to 2800 cm^{-1} [15] (region c)). Thus, the IR data unambiguously confirm the successful knitting of the aromatic building blocks with $-CH_2-$ moieties to form pristine HCPs (Figs. 1B and S4B). Additionally, for all polymers, the presence of a broad band in the region between 3700 and 3200 cm^{-1} can be observed, which is attributed to stretching vibration of the O−H bonds of water molecules entrapped in the HCPs network (region a; Fig. 1B). Trapping of water molecules in a polymer network was previously reported in several studies (e.g. [42,43]), and is usually observed as an effect of the post-synthesis purification process. However, it cannot be completely excluded that the bands in the range from 3700 to 3200 cm^{-1} result to some extent from the presence of hydroxyl (−OH) groups formed as by-products of Friedel-Crafts alkylation. This will be discussed in the following sections of the article.

As shown in Fig. S4A, new characteristic bands of $-SO_3H$ groups assigned to the asymmetric (centered at 1230 cm^{-1}; region e) and symmetric (centered at 1175 cm^{-1}; region f)

stretching vibrations of S=O bonds [15,44,45] emerged after the post-synthetic sulfonation of HCPs. A new band at 590 cm^{-1} (region g) is also observed and assigned to the stretching vibration of C-S bonds [32]. The presence of these bands confirms the successful post-functionalization of the HCPs with sulfonic groups (Fig. S4A).

The successful sulfonation of HCPs polymers was also confirmed by XPS data. As shown in Fig. 1C, for all sulfonated materials one can observe broad peak in S 2p region that can be deconvoluted into two spectral components at binding energy of ca. 169.9 and 168.7 eV. According to the literature [46–49], these two peaks are typical of spin-orbit components characteristic of S $2p_{1/2}$ and S $2p_{3/2}$ in sulfonic acid species ($-SO_3H$).

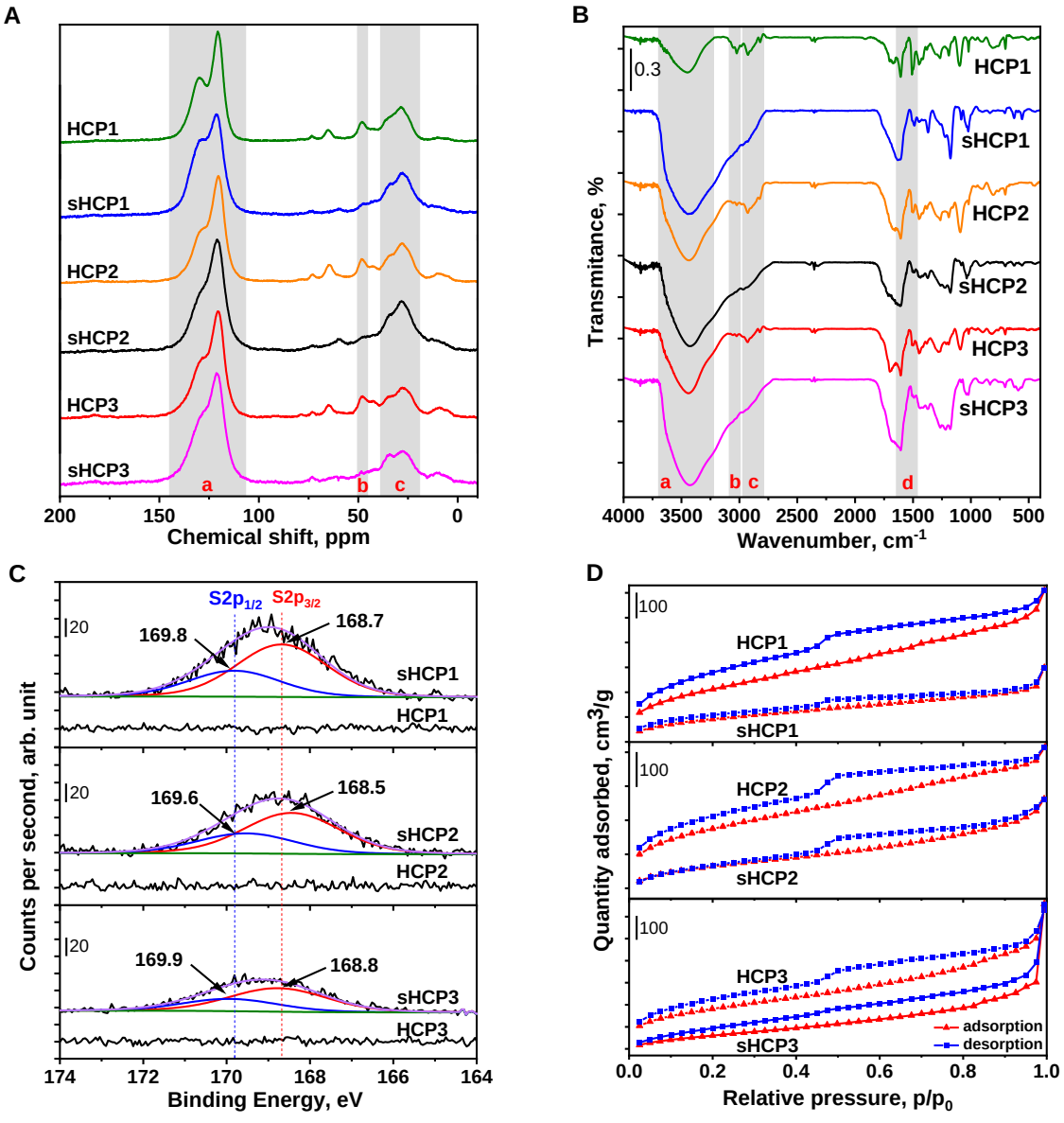

Fig. 1. (A) Solid-state CP/MAS ^{13}C NMR spectra of pristine and sulfonated HCPs (region a: aromatic carbons in TMP core, region b: sp^3 hybridized carbon of TPM and region c: aliphatic carbon derived from the cross-linker. (B) FTIR spectra of pristine and sulfonated HCPs (region a: stretching vibration of the O−H bonds of the $-SO_3H$ and –OH groups and/or water molecules entrapped within the HCPs network; region b: sp^2-hybridized C−H bonds of TPM core; region c: C−H bonds of sp^3-hybrized carbon of TPM core and methylene bridges; region d: stretching vibrations of C=C bonds of TPM core). (C) XPS spectra of the polymers in the S 2p energy range. (D) Low-temperature nitrogen adsorption-desorption isotherms of the investigated polymers.

No additional peaks were detected in S 2p region, indicating that the $-SO_3H$ functions were the only sulfur-containing species in the sulfonated polymers. Interestingly, the intensity of S 2p peaks was found to be proportional to the cross-linking density of the parent polymers. The higher the cross-linking density, the lower the intensity of the peaks typical of the $-SO_3H$ functions in materials obtained after post-synthetic sulfonation. This clearly indicates that there is some correlation between the TPM:FDA molar ratio used during the polymer synthesis and the efficiency of the post-synthesis sulfonation process.

The above-mentioned decrease in sulfonation efficiency at higher cross-linking density of the parent HCPs was further confirmed by elemental analysis (EA). As implied by the data in Table 1, sulfur content for sHCP1, sHCP2 and sHCP3 adsorbents was of 7.13, 4.74, and 3.82 wt%, respectively. This means that the efficiency of sulfonic acid species incorporation decreased by approximately 46% when the molar ratio of TPM:FDA increased from 1.0:4.5 to 1.0:13.5. It is very likely that lower sulfonation efficiency of the highly cross-linked polymers resulted from the presence of steric hindrance caused by the methylene bridges, that reduced availability of unoccupied positions of the aromatic TPM rings for electrophilic substitution of $-SO_3H$ groups. With respect to the results of the elemental analysis, it should be noted that all HCPs materials contained approximately 10-15 wt% of elements other than the expected C and

H (Table 1). A similar phenomenon was previously reported in references [31,41,50] and attributed to the formation of small amounts of chlorine and oxygen species (e.g. $–CH_2Cl$ and $–CH_2OH$ groups) as side products of Friedel-Crafts alkylation [27]. Loading of sulfonic acid species in sHCPs and ion exchange capacity of the polymers were also assessed using acid-base titration method [33]. As implied by data from Table S1, we observed good agreement between the sulfur content determined by elemental analysis and acid-base titration. Slightly higher values obtained by acid-base titration method were most likely due to the presence of some side products of Friedel-Crafts alkylation which are usually formed during the knitting process (e.g. $−CH_2OH$ or $−CH_2Cl$ groups [27]) and may take part in ion exchange process. In all pristine HCPs content of these side products was similar (ca. 0.19 mmol/g) and much lower than the sulfur loading (Table S1).

The morphology of all adsorbents was evaluated by scanning electron microscopy (SEM). HCPs were found to consist of rough agglomerates of irregular shape and size (Fig. 2), that form porous structure (Fig. S5). No significant morphological changes were observed with an increase of cross-linking density of the parent polymer networks, as well as after their post-synthetic sulfonation. The only noticeable change after post-synthetic sulfonation may be the smaller size of polymer aggregates (Fig. 2). This was most likely due to the disassembly of large aggregates into smaller ones under harsh sulfonation conditions. A similar phenomenon was also observed in other previous studies [51].

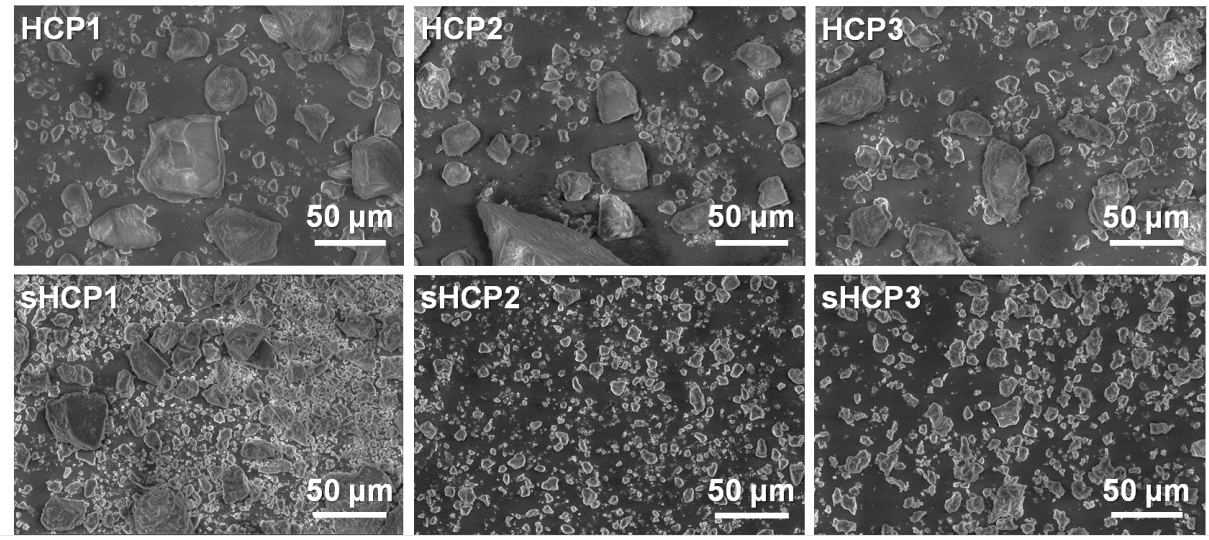

Fig. 2. SEM images of HCP1, HCP2, HCP3 (top panel), and their sulfonated counterparts sHCP1, sHCP2 and sHCP3 (bottom panel).

More precise information about the texture parameters of the adsorbents was provided by low-temperature nitrogen physisorption. As illustrated in Fig. 1D, all polymers exhibited a type IV(a) isotherm characteristic of mesoporous materials, in which capillary condensation is accompanied by hysteresis [52]. The same H4 type hysteresis loop was observed for all materials, indicating that cross-linking density had no significant impact on the porosity and pore structure of the triphenylmethane-based polymers [15,52]. The main textural properties of the analyzed materials are summarized in Table 1. Among the pristine HCPs, the highest BET surface area of 1061 m^2/g was observed for HCP1 characterized by the lowest cross-linking density. In the case of HCP2 and HCP3, BET surface areas were slightly lower (910 and 939 m^2/g, respectively), with similar average pore size (ca. 3.7-3.9 nm; Table 1). Considering porosity, it should be noted that all pristine polymers differed slightly in terms of pore size distribution. Increasing the cross-linking density resulted in slight broadening of pore size in pristine polymers. The higher the cross-linking density, the greater the contribution of mesopores of ca. 3.94 nm in size at the expense of pores of ca. 3.72 nm in diameter (Fig. S6). This effect resulted most likely from partial blockage of smaller mesopores by cross-linker.

Similar effect was also observed in other previous studies in this field [29]. As implied by the data in Table 1, post-synthetic sulfonation of HCPs resulted in a significant decrease in their BET surface area by approximately 40% compared to the pristine materials. A similar phenomenon was previously reported for various types of organic polymers after their post-synthetic sulfonation [15,32,44,47,53–55] and attributed to the partial blockage of pores by –SO_3H functions [56].

Table 1. Physicochemical characteristics of the polymers derived from nitrogen physisorption and elemental analysis.

Adsorbent	S_{BET}[a] [m^2/g]	CA[b] [°]	Average pore diameter[c] [nm]	Elemental composition[d] [wt%]		
				C	H	S
sHCP1	628	47 ± 0.1	3.72	63.63 ± 0.24	4.37 ± 0.02	7.13 ± 0.04
sHCP2	538	45 ± 0.1	3.72	65.19 ± 0.02	4.23 ± 0.05	4.74 ± 0.01
sHCP3	540	43 ± 0.1	3.72	67.26 ± 0.12	4.21 ± 0.01	3.82 ± 0.02
HCP1	1061	50 ± 0.1	3.72	84.32 ± 0.07	5.23 ± 0.06	n/a
HCP2	910	53 ± 0.1	3.72	78.68 ± 0.09	4.89 ± 0.09	n/a
HCP3	939	58 ± 0.1	3.94	79.52 ± 0.06	4.68 ± 0.03	n/a

[a] Specific surface area calculated using the BET model;

[b] Water contact angle derived from three to five measurements;

[c] Average pore diameter calculated from the desorption branch of the isotherms using the Barrett-Joyner-Halenda (BJH) method;

[d] Average values derived from three measurements determined based on EA.

The thermal stability of all materials was analyzed using TGA and the results are presented in Fig. S7A. No obvious mass loss of pristine polymers was observed upon heating up to approximately 300 °C. Most importantly, over 90 wt% of the polymers remained during heating in the 425-470 °C range (Fig. S7A) demonstrating that all parent materials prepared in this study exhibit a relatively high thermal stability. Post-synthetic sulfonation of pristine polymers, however, led to a slight decrease in their thermal stability (Fig. S7B). This is a very

common effect of the post-synthetic sulfonation and was previously observed for various organic materials [57]. For all TGA profiles of sulfonated polymers, a characteristic three-step degradation pattern can be observed, which is ascribed respectively to i) the desorption of trapped water in the polymer cages (ca. 5.0 wt%), ii) the decomposition of sulfonic acid groups, and iii) finally the destruction of the hydrocarbon network (Fig. S7B) [58].

Hydrophobicity/hydrophilicity of all polymers used in this study was evaluated by conducting water contact angle (CA) measurements (Table 1 and Fig. S8). It was found that CA values of the pristine HCP polymers differed slightly from each other, i.e. 50°, 53° to 58° for HCP1, HCP2 and HCP3, respectively, indicating the presence of a slightly hydrophilic polymer structures. Regarding the sulfonated polymers, it was documented that anchoring of the $–SO_3H$ groups on the polymer matrix reduced the contact angle of the pristine polymers revealing an increase in the hydrophilicity of these parent materials after the post-synthetic sulfonation. All sulfonated polymers exhibited comparable CA values in the range of 43-47° (Table 1). Regarding the hydrophilicity of polymers, it is essential to underline that the increase in hydrophilicity of the parent polymers after anchoring of sulfonic acid species was affected by the cross-linking density. The higher the cross-linking density, the higher the decrease in the CA value of the pristine polymer after its post-synthetic sulfonation (Table 1). The most pronounced decrease in the CA after the sulfonation process was observed for the material characterized by the highest cross-linking density (HCP3). In this case, CA value decreased from 58° for HCP3 to 43° for sHCP3, respectively (Fig. S8). Taking into account that hydrophilic properties of sHCPs result from the presence of sulfonic acid species, one would expect that a higher concentration of $–SO_3H$ groups in sHCP1 should result in their higher hydrophilicity when compared to sHCP3. However, this was not the case. This observation led to the conclusion that cross-linking density has significant impacted on localization of $–SO_3H$ groups in the polymer matrix. In the case of all polymers, post-synthetic sulfonation resulted in

anchoring of $–SO_3H$ groups both on the external surface of the polymer matrix and inside the pores. However, relatively low cross-linking density most probably facilitated a more efficient sulfonation of the polymer inside the pores resulting in a slightly lower concentration of sulfonic acid species on the external surface of the polymer and higher inside its pores. Since CA is a surface technique and a significant part of $–SO_3H$ groups in sHCP1 is localized inside the pores, the decrease in CA after the post-synthetic sulfonation was relatively small (only 3°, Fig. S8). In the case of sHCP3, higher cross-linking density promoted more efficient sulfonation of the polymers on the external surface of the polymer. This means that more $–SO_3H$ groups were localized on the external surface resulting in a higher decrease in CA after the post-synthetic sulfonation.

3.2. Antibiotic removal over the HCPs: adsorption capacity and kinetics

Preliminary adsorption tests were performed using ciprofloxacin, which is widely used as a model antibiotic pollutant and thus allows comparing the efficiency of materials used in this study with that of other previously reported adsorbents (see Section 3.5). It was found that all parent HCPs exhibited relatively low capability to adsorb CIP (less than 25% of the antibiotic removal in 180 min; Figs. 3 and S9-S10). The highest amount of the antibiotic was adsorbed on the material characterized by the highest cross-linking density (HCP3; Fig. 3). Adsorption capacity of this polymer was even higher than that observed for the commercial activated carbon (*Norit*), which is known from its strong capability to adsorb various organic pollutants, and is commonly used as a reference sample [59–62]. As shown in Fig. 3, post-synthetic sulfonation of the pristine polymers resulted in significant enhancement of their ability to adsorb the antibiotic. In contrast to the pristine HCPs, the highest efficiency of CIP removal was observed for sHCP1 characterized by the lowest cross-linking density and the highest $−SO_3H$ loading. In the case of sHCP2 and sHCP3, the efficiency of CIP removal was

significantly lower than that observed for sHCP1, but was still more than twice as that established for commercial activated carbon (Fig. 3).

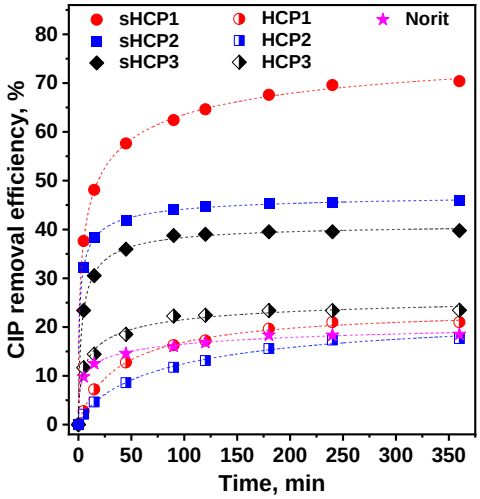

Fig. 3. Efficiency of ciprofloxacin removal in the presence of various adsorbents. *Adsorption conditions*: 200 mL of ciprofloxacin solution (C_0 = 15 mg/L), 5 mg of the polymer (adsorbent loading = 0.025 g/L), initial pH ~ 6.5 (before addition of the adsorbent), room temperature, stirring rate: 600 rpm.

Reactivity of the most efficient polymer was also evaluated at different adsorbent loadings and initial concentrations of the antibiotic. As illustrated in Figs. 4A and S11, at the lowest polymer loading (0.025 g/L) approximately 60% of the initial antibiotic dose was removed after 45 min of the adsorption process. When the amount of the adsorbent was doubled, more than 93% removal of CIP was after the same adsorption time. Further increasing the adsorbent concentration resulted in significant enhancement of the efficiency of the antibiotic removal. At the highest polymer loading (0.200 g/L), all of the antibiotic was effectively removed after just 5 min of the adsorption process (Figs. 4A and S11). This implies that the CIP removal efficiency and the time required to ensure successful removal of all antibiotic molecules from water can be simply adjusted by changing the adsorbent loading.

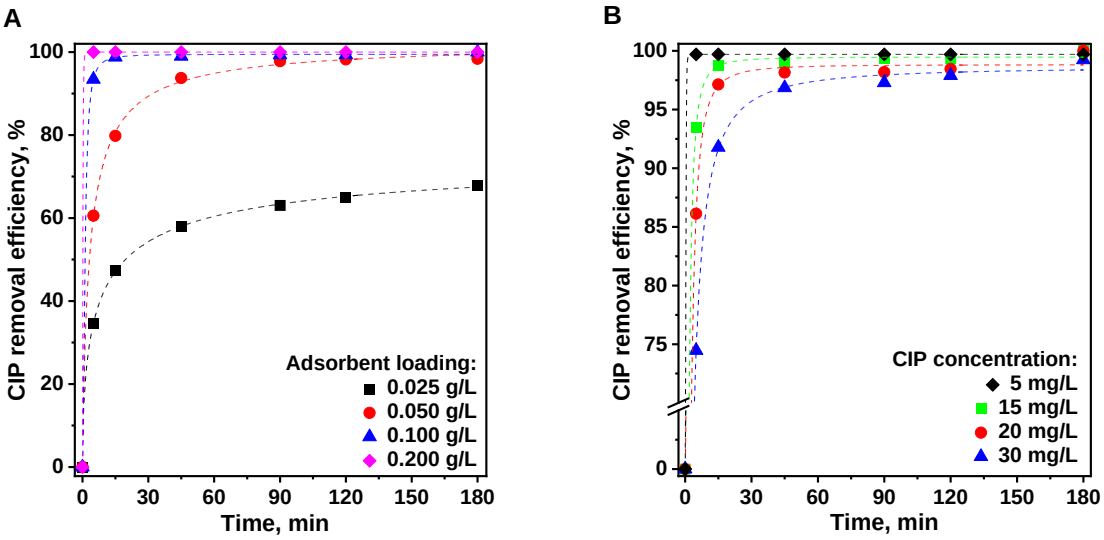

Fig. 4. (A) The effect of the sHCP1 loading on the efficiency of ciprofloxacin removal. *Adsorption conditions*: 200 mL of ciprofloxacin solution (C_0 = 15 mg/L), initial pH ~ 6.5 (before addition of adsorbent), room temperature, stirring rate: 600 rpm. (B) The effect of initial ciprofloxacin concentration on its removal in the presence of sHCP1. *Adsorption conditions*: 200 mL of CIP solution, 20 mg of the polymer (adsorbent loading = 0.100 g/L), initial pH ~ 6.5 (before addition of the adsorbent), room temperature, stirring rate: 600 rpm.

Concerning the effect of initial concentration of the antibiotic, it was established that a relatively small amount of the polymer (0.100 g/L) enables very efficient elimination of CIP from water over a wide concentration range (from 5 to 30 mg/L). As shown in Figs. 4B and S12, at the lowest CIP concentration all antibiotic pollutant was removed after just 5 min of the adsorption process. Furthermore, the efficiency of CIP removal was only slightly reduced when CIP concentration increased from 5 to 30 mg/L. Even at the highest concentration of CIP more than 97% of initial antibiotic dose was successfully removed after 45 min of the adsorption process. Thus, the above-mentioned experiments clearly show that the efficient CIP removal in the presence of a very small quantity of sHCP1 adsorbent is not limited only to very low

concentrations of the antibiotic pollutant, and the polymer can successfully remove antibiotic molecules over its wide concentration range.

To gain more detailed information on the mechanism and kinetics of the adsorption process, the experimental data were fitted to pseudo-first order (PFO) and pseudo-second order (PSO) models proposed by Ho and McKay [63]. Based on the results shown in Table 2, it was determined that the experimental data obtained for all sulfonated polymers fit more into the PSO than PFO model. For the former, the R^2 values were higher than 0.999 and experimentally derived q_e values were very close to the calculated ones (Fig. S13). This clearly indicates that the rate-determining step of the adsorption process over the sulfonated polymers is a chemical reaction between adsorbent and adsorbate (chemisorption) [14,32]. Among all polymers, the highest adsorption capacity was observed for sHCP1, and was approximately 4 times higher than the capacity estimated for the commercial activated carbon (427.5 vs. 110.5 mg/g, respectively; Table 2), and approximately 1.5 times higher than that determined for sHCP2 and sHCP3 (Table 2).

Table 2. CIP adsorption kinetic parameters derived from the pseudo-first order (PFO) and pseudo-second order (PSO) models [34]. Representative graphs used for estimating of the adsorption kinetics are shown in Figs. S14-S16.[a]

Adsorbent	q_e (exp)[b] [mg/g]	PFO			PSO		
		k [1/min]	q_e (cal)[c] [mg/g]	R^2	k [g/mg/min]	q_e (cal)[c] [mg/g]	R^2
sHCP1	427.5	0.01700	226.8	0.92429	0.00026	436.7	0.99940
sHCP2	272.1	0.02488	100.5	0.95378	0.00112	274.7	0.99995
sHCP3	236.3	0.03328	125.8	0.97475	0.00108	239.2	0.99994
HCP1	128.9	0.01443	113.7	0.98699	0.00019	143.9	0.99841
HCP2	105.3	0.01476	112.7	0.94595	0.00015	122.1	0.99409
HCP3	139.2	0.02574	93.3	0.95197	0.00083	143.3	0.99947
Norit	110.5	0.02222	75.5	0.91849	0.00084	113.6	0.99874

[a] *Adsorption conditions*: 200 mL of CIP solution (C_0 = 15 mg/L), 5 mg of the polymer (adsorbent loading = 0.025 g/L), initial pH ~ 6.5 (before addition of the adsorbent), room temperature, stirring rate: 600 rpm.

[b] Maximum adsorption capacity of the sample derived from the experiments.

[c] Maximum adsorption capacity of the sample calculated based on a given kinetic model.

To shed more light on the nature of adsorption sites on the surface of sHCP1 polymer (the most effective adsorbent), additional adsorption tests were conducted at different initial pH values. The basic hypothesis was that different speciation of CIP at various pH would provide more accurate information about the nature of interaction between adsorbent and adsorbate. As shown in Figs. 5A and S17, the highest efficiency of CIP removal was observed at initial pH close to neutral when the antibiotic exists in the zwitterionic form [64]. In strongly acidic conditions, where CIP molecules are positively charged (Fig. S18) [64], the efficiency of CIP removal was only slightly reduced compared to neutral conditions. Interestingly, the lowest efficiency of CIP adsorption was observed under strongly alkaline conditions (pH ~ 11.4) at which the antibiotic exists only in anionic form [64]. After 180 min of adsorption process under such strong alkaline conditions the efficiency of CIP removal was reduced by almost 90% (compared to native pH), and only ca. 10% of the initial antibiotic dose was adsorbed on sHCP1 (Fig. 5A). Since the surface of sHCP1 was charged negatively over the entire pH range investigated in this work (see zeta potential measurements in Fig. S19), it is clear that the strongly enhanced adsorption capacity of the sulfonated polymers at pH close to 6.5 and 2.5 was mainly due to the ionic interaction between the protonated secondary amine group of piperazine moiety of CIP molecules and the negatively charged sulfonic acid groups on the polymer surface. The proposed mechanism of CIP adsorption via ionic interactions is also consistent with very low efficiency of CIP removal on sHCP1 polymer under strongly alkaline conditions (pH ~ 11.4), where CIP molecules are negatively charged (deprotonated carboxyl groups and non-protonated the secondary amine group). Thus, the strong electrostatic repulsion

between negatively charged CIP molecules and negatively charged sulfonic acid species on sHCP1 polymer is expected to hinder efficient adsorptive removal of the antibiotic. The hypothesis of the key role of surface sulfonic acid species in the strongly enhanced removal of CIP on sHCP materials via chemisorption was further confirmed by the presence of a clear linear correlation between the concentration of $-SO_3H$ groups in the sulfonated polymers and their adsorption capacity (Fig. 5B).

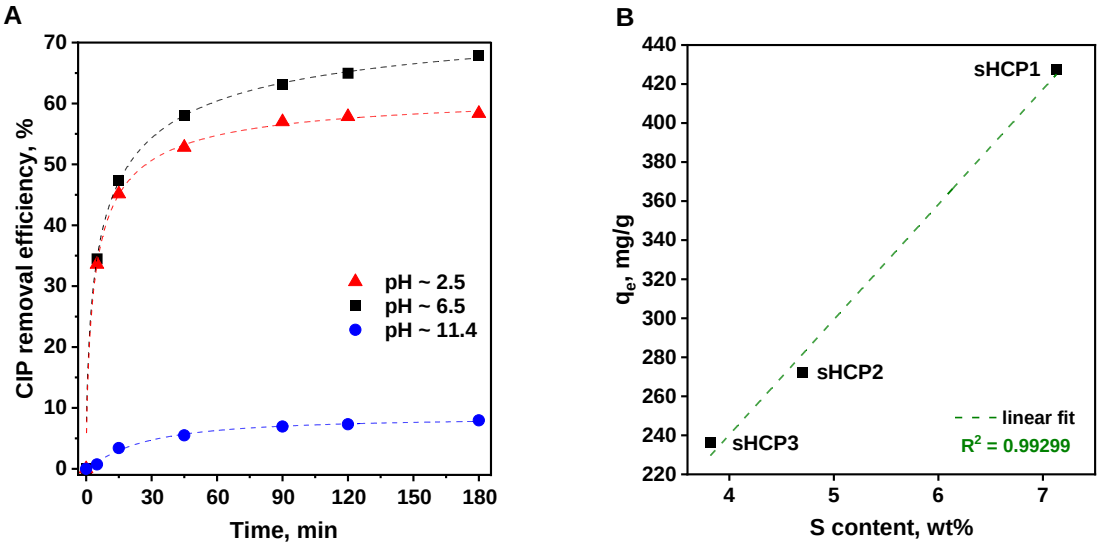

Fig. 5. (A) The effect of initial pH values on the ciprofloxacin removal in the presence of sHCP1. *Adsorption conditions*: 200 mL of CIP solution (C_0 = 15 mg/L), 5 mg of the polymer (adsorbent loading = 0.025 g/L), room temperature, stirring rate: 600 rpm. (B) The relationship between sulfur content in the investigated adsorbents and their adsorption capacity toward CIP at pH close to neutral (pH ~ 6.5).

In view of all these results, one can clearly conclude that the $-SO_3H$ functions are the key species that play decisive role in the strongly enhanced adsorptive removal of this antibiotic pollutant on the surface of sulfonated HCPs. Even though the surface area of the pristine polymers was decreased by approximately 40% after their post-synthetic sulfonation (Table 1), the sulfonated materials still exhibited significantly higher efficiency in CIP adsorption than

the pristine polymers (Table 2). Based on the above, we can also clearly state that significantly less efficient adsorption of the antibiotic on the surface of the pristine HCPs resulted mainly from different surface properties of these materials. Indeed, as implied by zeta potential measurements, the surface of the pristine HCP1 polymer was close to neutral at pH ~ 6.5 (Fig. S19). Therefore, CIP molecules existing in its zwitterionic form could not be adsorbed efficiently through ionic interactions. The most probable adsorption mechanism for the parent HCPs is, thus, the formation of the conjugated system between the aromatic rings of both the polymer network and the adsorbate molecule that favors CIP adsorption via π-π stacking. Among all pristine HCPs, the highest adsorption capacity was observed for HCP3, which surface was the most hydrophobic (Table 1), promoting more efficient adsorption of the antibiotic via π-π stacking. The possible contribution of –OH groups as side products of Friedel-Crafts alkylation to the most efficient adsorption of CIP on HCP3 can be excluded, as all pristine polymers exhibited comparable ion exchange capacity (Table S1). A similar mechanism of antibiotics adsorption on the surface of the pristine hyper-cross-linked polymers via π-π stacking was proposed in previous studies [43,51,65]. However, this adsorption mechanism was found to be significantly less efficient in terms of elimination of CIP than the ionic interaction because of the polar properties of the model antibiotic pollutant. The possible mechanism of CIP adsorption on sHCP1, proposed based on experimental data obtained in this study, is schematically shown in Fig. 6. This adsorption mechanism assuming a strong interaction between sulfonic acid species on polymer matrix and protonated antibiotic molecules was further confirmed by FTIR-ATR measurements. As shown in Fig. S20, IR spectrum of sHCP1 after CIP adsorption reveals the presence of vibrational bands characteristic for both fresh sHCP1 and CIP. However, it can be readily observed that the key band at 1628 cm^{-1} attributed to N–H bending vibration in amine group in the piperazine moiety of adsorbed CIP [66] was clearly shifted toward higher wavenumbers when compared to powdered CIP. This confirms

the presence of strong interactions between amine functional group of the antibiotic and sHCP1 network. This strong interaction between amine species in CIP molecules and –SO_3H groups in the polymer was also confirmed by XPS. As shown in Fig. S21, S 2p peak characteristic of –SO_3H species in sHCP1 was shifted significantly toward lower binding energy values after CIP adsorption. This was associated with a significant shift of N 1s peak typical of amine group in CIP molecules toward higher energy values after antibiotic adsorption when compared to CIP. Thus, XPS studies led us to confirm that these two functional groups strongly interacts leading to increase in electron density in the neighborhood of sulfur in –SO_3H groups and decrease in electron density of nitrogen atom in amine group of CIP. As for the adsorption mechanism, it should be underlined that slight increase in binding energy of fluorine species in adsorbed CIP was also observed. This may indicate that this halogen also takes part, to some extent, in the antibiotic adsorption via physical interactions (e.g. hydrogen bonding) with the polymer matrix.

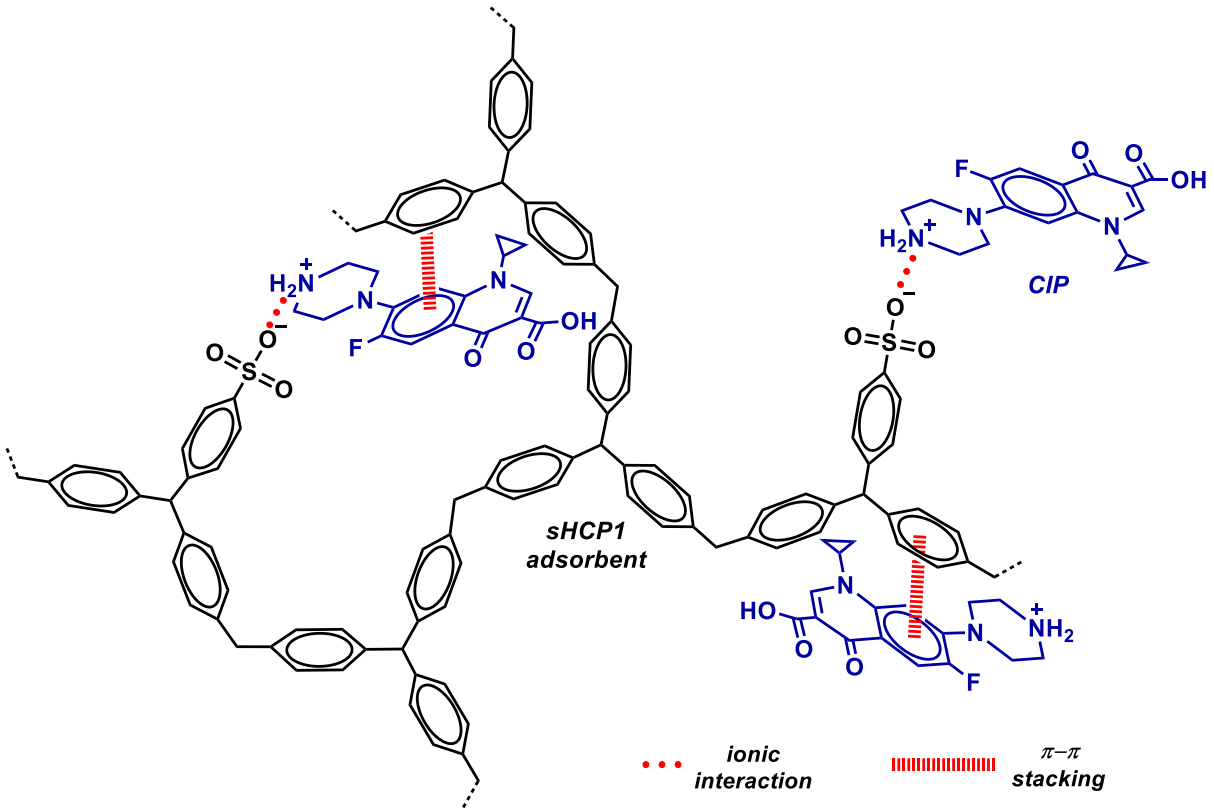

Fig. 6. Schematic representation of the possible mechanisms of CIP adsorption on sHCP1 polymer elucidated on the basis of experimental data.

More detailed studies aiming at precise analysis of the adsorption mechanism, Gibbs free energy (ΔG^0), activation energy (E_a) and adsorption isotherms were established for the most efficient adsorbent (sHCP1). According to the results, ΔG^0 value at 20 °C was found to be of –32.25 kJ/mol. This implies that adsorption of CIP on sHCP1 occurred feasibly and spontaneously [38]. Analysis of the estimated Gibbs free energy change led also to determination of the nature of interaction between adsorbent and adsorbate. According to literature [67], ΔG^0 values lower than –20 kJ/mol indicate adsorption of pollutants via physical processes, while for chemisorption they should range from –80 to –400 kJ/mol. In this work, ΔG^0 was between the values characteristic for physisorption and chemisorption suggesting that adsorption of CIP on sHCP1 involved both physical adsorption and chemisorption [68]. To shed more light on the nature of interaction between adsorbent and adsorbate, activation energy (E_a) was estimated based on Arrhenius equation (see Fig. S22). According to literature [69], physical adsorption process has lower E_a values (5−40 kJ/mol) when compared to chemical ones (40−800 kJ/mol). In this work, E_a value was estimated to be 41.22 kJ/mol indicating that CIP was adsorbed on sHCP1 mainly via chemisorption. Moreover, positive value of E_a indicated that adsorption process was endothermic and favored at higher temperatures [70]. The latter was also confirmed by higher rate of CIP adsorption at elevated temperatures (Figs. S23 and S24). Decisive role of chemisorption in antibiotic removal on sHCP1 was also confirmed by fitting of experimental data to Langmuir and Freundlich isotherm models (Fig. S25 and Table S2). According to the results, Langmuir model better describes the adsorption behavior implying that CIP was mainly adsorbed on a specific and uniform positions resulting in formation of single layer coverage of the antibiotic on sHCP1 polymer. This further confirms that adsorption of CIP over sHCP1 proceeds mainly via ionic interactions between the adsorbate and sulfonic acid species on the polymer surface. Based on all these results, we established that adsorption of CIP on sHCP1 resulted both from physical and chemical interactions between the

adsorbate and adsorbent, but the contribution of chemisorption to removal of the antibiotic was dominant.

To identify and elucidate dynamics of various steps of the adsorption process over sHCP1, experimental data were also fitted to Weber-Morris intraparticle diffusion (ID) model [71]. As shown in Fig. S26, we did not observe only one linear region passing through the coordinate origin. This implies that the intraparticle diffusion was not the only rate determining step of the adsorption process and CIP adsorption on sHCP1 is more complex phenomena. Instead, we observed three distinct stages of linearity. The first step was the fastest (k_1 = 76.097 mg g^{-1} $min^{-1/2}$) and attributed to the film diffusion, in which the adsorbate is transferred from the bulk solution to the boundary layer surrounding adsorbent's particles. In this step, adsorbate was adsorbed mainly on external surface area of the polymer. The second step was found to be significantly slower (k_2 = 8.934 mg g^{-1} $min^{-1/2}$) and most likely resulted from intraparticle diffusion, in which the adsorbate diffuses through the internal pores of the adsorbent by pore diffusion (diffusion through the pore water) and/or surface diffusion (diffusion of adsorbed ions/molecules onward the adsorbent's internal surface). In the third and the slowest step (k_3 = 2.176 mg g^{-1} $min^{-1/2}$), the adsorbent molecules diffused from larger pores to the smaller ones and this resulted in a slow adsorption rate.

3.3. Versatility of sHCP1

Potential application of various adsorbents is often limited by their versatility. The present study investigated this feature of sHCP1 polymer by evaluating its adsorption capacity toward other commonly prescribed antibiotics of different structures, namely amoxicillin, sulfamethoxazole and tetracycline. The structure and basic physicochemical properties of these pharmaceuticals are displayed in Table S3. As shown in Figs. 7A and S27, the TC removal efficiency in the presence of sHCP1 polymer was comparable to that observed for CIP removal (q_e = 413.2 mg/g vs. 427.5 mg/g, respectively). In contrast, the ability of sHCP1 polymer to

adsorb SMX and AMX model pollutants was found to be slightly lower (Figs. 7A and S27, and Table S4). This may result from different structures of the two antibiotics and steric hindrance in the neighborhood of amine groups, which are responsible for adsorption of the antibiotics via ionic interactions. It is very likely that presence of other functional groups in a close proximity of antibiotic molecules and/or stearic hindrance may have significant impact on the strength of ionic interactions between the adsorption sites of sulfonated polymers and the protonated amine group of the adsorbate (antibiotic molecules). Regarding the adsorption kinetics, experimental data collected during the removal of SMX, AMX and TC fit the PSO model very well (Table S4 and Fig. S28). For all these pharmaceuticals, the adsorption capacities obtained experimentally and theoretically based on this model were in good agreement (Fig. 7B). It implies that all of these pollutants were most likely adsorbed on sHCP1 via ionic interaction between the protonated functional group of respective antibiotic and the negatively charged sulfonic acid functions in the polymer network (chemisorption). Moreover, it clearly indicates that sHCP1 is a versatile adsorbent which enables efficient removal of various antibiotics when present in zwitterionic or cationic form.

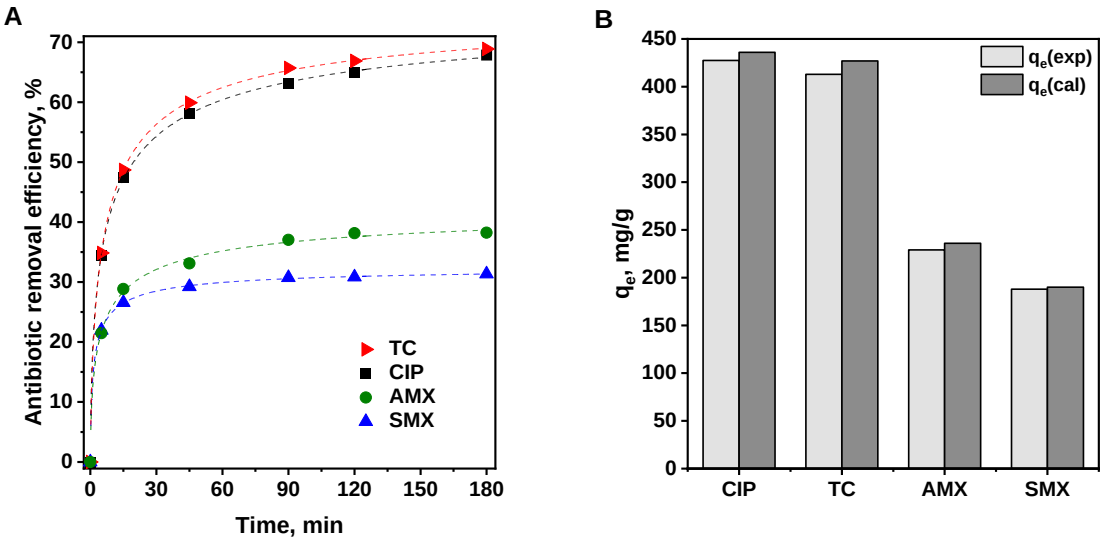

Fig. 7. (A) Efficiency of the antibiotics removal by sHCP1 as a function of the adsorption time. (B) Comparison of a maximum adsorption capacity of sHCP1 adsorbent toward the selected

antibiotics derived from experimental data (q_e(exp)), and calculated from the PSO kinetic model (q_e(cal)). *Adsorption conditions*: 200 mL of antibiotic solution (C_0 = 15 mg/L), 5 mg of the polymer (adsorbent loading = 0.025 g/L), room temperature, initial pH ~ 6.5, stirring rate: 600 rpm.

As mentioned above, sHCP1 can efficiently adsorb various antibiotics from a single-component mixture. However, it is not clear how it will work with multicomponent mixture of antibiotic pollutants. In other words, it is not clear whether the adsorption of one pollutant will enhance or diminish efficiency of sHCP1 in adsorption of other antibiotics. To shed more light on the affinity of the sulfonated polymer toward selected antibiotics, additional experiments were performed with the use of ternary mixtures containing equimolar amounts of ciprofloxacin, tetracycline and sulfamethoxazole (initial concentration of SMX, TC and CIP = 45.27 μmol/L). The efficiency of antibiotics removal from ternary mixture was determined by means of LC-MS analyses (Fig. 8B) and compared to that observed for monocomponent antibiotic solutions containing the same concentration of CIP, SMX and TC (Fig. 8A). According to the results, the highest efficiency of antibiotics removal from monocomponent solutions was observed for CIP (Fig. 8A). Under the same conditions, SMX and TC were removed significantly less efficient. This shows that structure of CIP is the most favorable for efficient adsorption on sHCP1 polymer. The same conclusions were drawn based on experimental data obtained for ternary mixture of antibiotics. As shown in Fig. 8B, all antibiotics could be adsorbed on sHCP1 from such multicomponent solution, but the highest efficiency of antibiotic removal was observed for CIP. After 180 min, approximately 30% of the initial CIP dose was removed, while TC and SMX were removed with efficiencies lower than 5%. Significantly lower efficiency of CIP removal from the ternary mixture than that observed for the monocomponent solution shows that some of the adsorption sites on sHCP1 were occupied by TC and SMX, diminishing availability of the adsorption sites for CIP. The same is true also for SMX and TC. In view of

these results, one can conclude that adsorption of one antibiotic on sHCP1 hinders further adsorption of others on the same adsorption sites. Thus, all antibiotics selected in this study exhibit comparable affinity to the adsorption sites on sHCP1. In other words, none of the antibiotics selected in this work is adsorbed more efficient from the ternary mixture at the expense of the others.

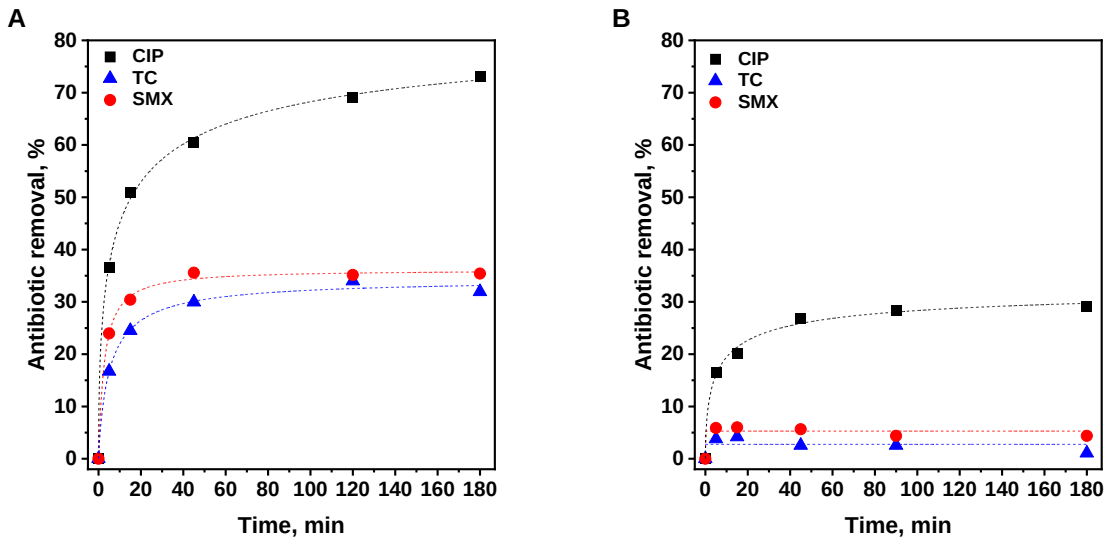

Fig. 8. (A) Efficiency of antibiotics removal from monocomponent solutions containing the same molar concentration of CIP, SMX or TC. (B) Efficiency of antibiotics removal from ternary mixture containing equimolar amount of CIP, SMX and TC. *Adsorption conditions*: 200 mL of antibiotic mixture (initial concentration of SMX, TC and CIP = 45.27 μmol/L), initial pH ~ 6.5 (before addition of the adsorbent), 5 mg of the polymer (adsorbent loading = 0.025 g/L), room temperature, stirring rate: 600 rpm.

Results obtained in this study showed that antibiotics are adsorbed on sHCP1 mainly through ionic interactions. To evaluate the influence of other ions in water matrices on the efficiency of CIP adsorption on sHCP1, we performed additional experiments with more complex matrices. We considered two scenario in which antibiotic was dissolved in tap water and river water (for more details please see experimental section). The former sample contains

significant amount of cations and anions that are present in tap water at much higher quantity than CIP, and may hinder effective adsorption of the antibiotic on the polymer via ionic interactions. The latter sample contains not only cations and anions but also dissolved organic matter.

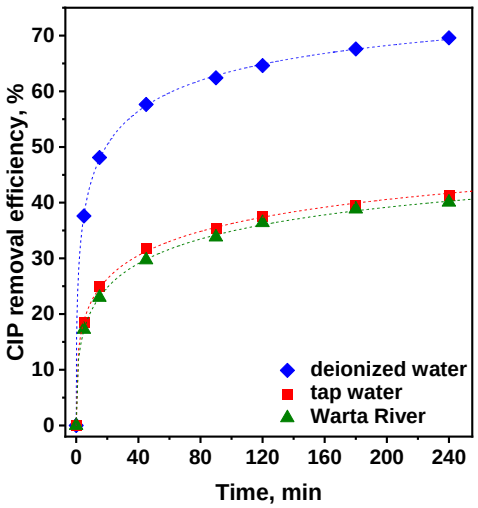

Fig. 9. Efficiency of ciprofloxacin removal from deionized water, tap water and Warta River in the presence of sHCP1 adsorbents. *Adsorption conditions*: 200 mL of ciprofloxacin solution (C_0 = 15 mg/L), 5 mg of the polymer (adsorbent loading = 0.025 g/L), initial pH ~ 7.0-6.5 (before addition of the adsorbent), room temperature, stirring rate: 600 rpm.

As shown in Fig. 9, the efficiency of CIP removal from tap water and river water was approximately 40% lower when compared with deionized water, but still relatively high amount of the antibiotic could be removed in the presence of sHCP1 adsorbent. This shows that various ions and organic matter may reduce the efficiency of CIP removal on sHCP1, but do not hinder its potential application for remediation of antibiotics from real environmental matrices.

3.4. Regeneration and reuse of sHCP1

Along with versatility, regeneration of the adsorbents is another important parameter limiting their practical application. In this study, this feature of sHCP1 polymer was evaluated

by conducting a series of ten subsequent adsorption cycles followed by regeneration steps with the use of aqueous solution of hydrochloric acid as regeneration agent (experimental details are described in Section 2.6). As shown in Figs. 10A and S29A, no noticeable decrease in the efficiency of sHCP1 was observed after 10 adsorption cycles, indicating high reusability and long-term stability of the sulfonated polymer. High chemical stability of the reused polymer was also confirmed by FTIR studies. As shown in Fig. S29B, there were no significant differences in the structure of fresh sHCP1 adsorbent and material after ten reuse tests. It is important to emphasize that previously reported SO_3H-functionalized polymers rarely displayed such high stability after so many adsorption cycles. Usually, significant decrease in their efficiency was observed after 4^{th} or 5^{th} adsorption cycle [47,53,54,57,72–74]. Thus, results obtained in this work clearly indicate that the hyper-cross-linked polymers are promising supports for anchoring of sulfonic acid species that enable simple and efficient incorporation of these functional groups to the polymer network, and ensure their high stability both under working conditions and during the adsorbent regeneration process. Regarding the regeneration of the spent adsorbent, it is important to underline that significantly lower efficiency of regeneration was observed when ethanol was used instead of hydrochloric acid as regeneration agent (see Fig. S30). This further confirmed that CIP was mainly adsorbed via chemical interactions (chemisorption) rather than physical ones [38].

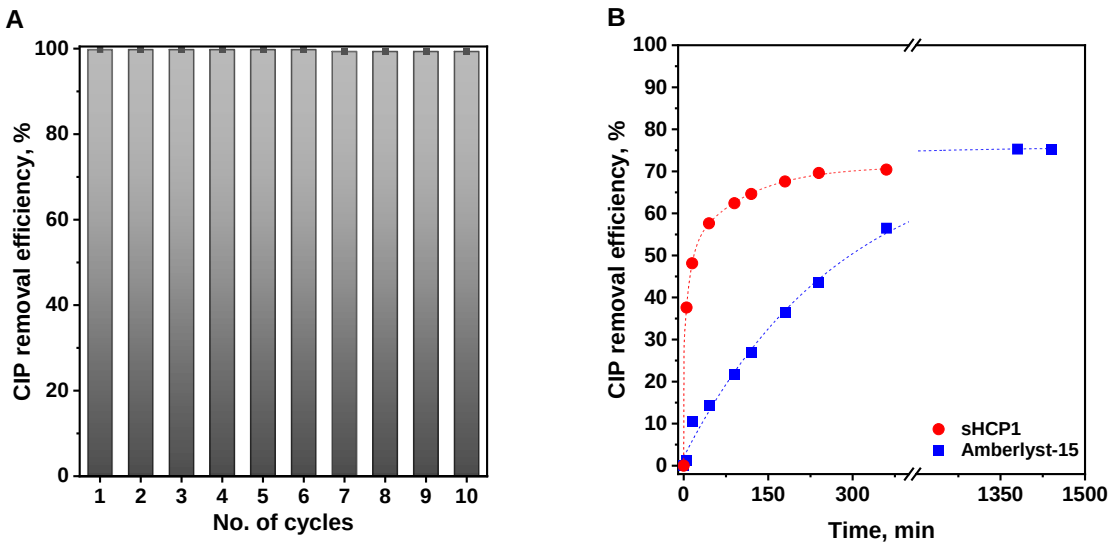

Fig. 10. (A) Stability of sHCP1 polymer during 10 adsorption-desorption cycles. *Adsorption conditions*: 200 mL of ciprofloxacin solution (C_0 = 15 mg/L), 20 mg of adsorbent (adsorbent loading = 0.100 g/L), room temperature, initial pH ~ 6.5, stirring rate: 600 rpm. Regeneration procedure is described in experimental section. (B) Efficiency of ciprofloxacin removal in the presence of sHCP1 and *Amberlyst-15*. *Adsorption conditions*: 200 mL of ciprofloxacin solution (C_0 = 15 mg/L), 5 mg of the polymer (polymer loading = 0.025 g/L), initial pH ~ 6.5 (before addition of the polymer), room temperature, stirring rate: 600 rpm.

3.5. Comparison of sHCP1 with previously reported adsorbents

The results obtained in this study demonstrate that sHCP1 significantly outperforms commercial activated carbon (*Norit*) in terms of its efficiency in CIP removal (q_e = 427.5 vs. 110.5 mg/g, respectively). A more thorough literature search also indicated that sHCP1 is more efficient than other previously reported adsorbents, such as chitosan-based materials (22.7 mg/g [75], 36.7 mg/g [76]), agriculture waste (92.4 mg/g [77]), covalent organic polymer (84.0 mg/g [78]) or graphene hydrogel (235.6 mg/g [79]) (Table S5). It is noteworthy that the adsorption capacity of sHCP1 was found to be comparable to that established for organically modified bentonite (427.5 vs. 457.0 mg/g respectively [80]), which is the most efficient adsorbent in the

comparison presented in Table S5. Comparing with other previously used adsorbent for TC removal, sHCP1 synthesized in this study showed much higher adsorption capacity than agriculture waste-coated zinc oxide (98.7 mg/g [77]), zeolites (201.8 mg/g [81], 303.3 mg/g [82]), zeolitic imidazolate framework-8 (312.5 mg/g [13]), as well as HCPs with other functional groups (209.0 mg/g [15], 268.1 mg/g [83], 273.2 mg/g [51]; more examples are provided in Table S5). As for the efficiency of adsorptive removal of other antibiotics, the estimated adsorption capacity of sHCP1 toward AMX (228.9 mg/g) and SMX (188.1 mg/g) was higher or comparable to the adsorption capacity of adsorbents reported in the literature (Table S5). For instance, sHCP1 exhibited a higher adsorption capacity toward AMX than agriculture waste (132.2 mg/g [77]) and comparable capacity to modified montmorillonite K10 (215.1 mg/g [84]), metal-organic framework MIL-53(Al) (258.4 mg/g [85]) and also other porous polymers (208.6 mg/g [86]).

Concerning the adsorption efficiency of sHCP1, it should be noted that the most promising sulfonated polymer synthesized in this work exhibited similar adsorption capacity to commercial *Amberlyst-15* (427.5 vs. 466.0 mg/g, respectively; Fig. 10B) which possess approximately twice the loading of sulfonic acid species (Table S1). The great advantage of the polymers synthesized in this work may also be considered in terms of kinetics of CIP removal. As shown in Fig. 10B, sHCP1 enabled much faster elimination of the antibiotic than *Amberlyst-15*. This was most likely due to much larger surface area and porosity of the former sample that enabled more efficient adsorption of CIP in a much shorter adsorption time (BET surface area of *Amberlyst-15* = 43 m^2/g [87] vs. 628 m^2/g for sHCP1). Based on above, one can clearly conclude that sHCP1 is a promising polymer-based sulfonated adsorbent for fast and efficient elimination of antibiotic pollutants from water, and presents great advantage over other commercial nanomaterials (*Norit* and *Amberlyst-15*).

4. Conclusions

Results obtained in this work showed that sulfonated hyper-cross-linked polymers are promising adsorbents for fast, efficient and reversible adsorption of antibiotic pollutants from water. Their adsorption capacity is inversely proportional to the cross-linking density of the parent HCPs and directly proportional to the loading of $-SO_3H$ in the polymer network. The main adsorption mechanism over sulfonated HCPs is chemisorption of the pollutant via ionic interactions. The most promising polymer (sHCP1) exhibited approximately 4 times higher adsorption capacity toward CIP than that observed for the commercial carbon-based adsorbent (*Norit*), and enabled much faster elimination of the antibiotic than commercial sulfonated polymer (*Amberlyst-15*). As concerns the versatility of the HCPs-based adsorbents, it was documented that sHCP1 can efficiently remove polar antibiotic pollutants from both single and ternary mixtures. The highest affinity of the adsorbent was observed for ciprofloxacin, followed by sulfamethoxazole and tetracycline. Moreover, sHCP1 exhibited outstanding regeneration during ten subsequent adsorption–desorption cycles.

We firmly believe that results obtained in this work not only outline great potential of the sulfonated HCPs-based nanomaterials as promising adsorbents for the efficient removal of polar antibiotic pollutants. It is expected that fundamental knowledge resulting from this work may allow to reduce costs related to the synthesis of HCPs-based adsorbents due to lowering the consumption of the cross-linking agents and corrosive $FeCl_3$ catalyst. Since the latter is usually used in equimolar amount in respect to the cross-linking agent, our findings may have significant importance not only for the cost-effectiveness of the polymer synthesis but also protection of the environment.

Acknowledgments

National Science Centre, Poland (NCN) (Grant No. 2022/06/X/ST5/00222) is acknowledged for the financial support of this work. L. Wolski gratefully acknowledges the Polish Minister of Education and Science (decision no. SMN/16/0997/2020) for scholarship. Dr. Eng. Łukasz

Majchrzycki (Center for Advanced Technology, Adam Mickiewicz University, Poznań) is acknowledged for his help in conducting zeta potential measurements. I. Telegeiev and M. El-Roz thanks the French hosting program (PAUSE) and Caen University for the financial support.

Author contributions

J.W.: conceptualization, methodology, validation, investigation, resources, data curation, writing – original draft and review, funding acquisition, project administration; M.M.: investigation (TGA analysis), writing – review and editing; I.T.: investigation (CP/MAS ^{13}C NMR analysis), writing – review and editing; H.E.: investigation (CP/MAS ^{13}C NMR analysis), writing – review and editing; M.F.: investigation (LC-MS analysis), writing – review and editing; A.S.: investigation (CA analysis), writing – review and editing; J.W.-K.: writing – review and editing; M.E-R.: writing – review and editing; L.W.: conceptualization, methodology, writing – original draft and review, supervision.

Competing interests

The authors declare no competing interests.

Appendix A. Supplementary data

Supplementary data associated with this article can be found online.

References

[1] A.J. Browne, M.G. Chipeta, G. Haines-Woodhouse, E.P.A. Kumaran, B.H.K. Hamadani, S. Zaraa, N.J. Henry, A. Deshpande, R.C. Reiner, N.P.J. Day, A.D. Lopez, S. Dunachie, C.E. Moore, A. Stergachis, S.I. Hay, C. Dolecek, Global antibiotic consumption and usage in humans, 2000–18: a spatial modelling study, Lancet Planet. Heal. 5 (2021) e893–e904. https://doi.org/10.1016/S2542-5196(21)00280-1.

[2] Y. Yang, W. Song, H. Lin, W. Wang, L. Du, W. Xing, Antibiotics and antibiotic resistance genes in global lakes: A review and meta-analysis, Environ. Int. 116 (2018) 60–73. https://doi.org/10.1016/j.envint.2018.04.011.

[3] J.L. Wilkinson, A.B.A. Boxall, D.W. Kolpin, K.M.Y. Leung, R.W.S. Lai, D. Wong, R. Ntchantcho, J. Pizarro, J. Mart, S. Echeverr, J. Garric, A. Chaumot, P. Gibba, I. Kunchulia, S. Seidensticker, G. Lyberatos, H. Morales-salda, Jorge Manuel Kang, Pharmaceutical pollution of the world's rivers, Proc. Natl. Acad. Sci. U. S. A. 119 (2022) e2113947119. https://doi.org/10.1073/pnas.2113947119.

[4] S.M. Al-Jubouri, H.A. Al-Jendeel, S.A. Rashid, S. Al-Batty, Antibiotics adsorption from contaminated water by composites of ZSM-5 zeolite nanocrystals coated carbon, J. Water Process Eng. 47 (2022) 102745. https://doi.org/10.1016/j.jwpe.2022.102745.

[5] A.A. Aryee, R. Han, L. Qu, Occurrence, detection and removal of amoxicillin in wastewater: A review, J. Clean. Prod. 368 (2022) 133140. https://doi.org/10.1016/j.jclepro.2022.133140.

[6] M. Ahmed, M.O. Mavukkandy, A. Giwa, M. Elektorowicz, E. Katsou, O. Khelifi, V. Naddeo, S.W. Hasan, Recent developments in hazardous pollutants removal from wastewater and water reuse within a circular economy, Npj Clean Water. 5 (2022) 1–25. https://doi.org/10.1038/s41545-022-00154-5.

[7] B.L. Phoon, C.C. Ong, M.S. Mohamed Saheed, P.L. Show, J.S. Chang, T.C. Ling, S.S. Lam, J.C. Juan, Conventional and emerging technologies for removal of antibiotics from wastewater, J. Hazard. Mater. 400 (2020) 122961. https://doi.org/10.1016/j.jhazmat.2020.122961.

[8] B.K. Biswal, R. Balasubramanian, Adsorptive removal of sulfonamides, tetracyclines and quinolones from wastewater and water using carbon-based materials: Recent developments and future directions, J. Clean. Prod. 349 (2022) 131421. https://doi.org/10.1016/j.jclepro.2022.131421.

[9] K. Azam, N. Shezad, I. Shafiq, P. Akhter, F. Akhtar, F. Jamil, S. Shafique, Y.-K. Park, M. Hussain, A review on activated carbon modifications for the treatment of wastewater containing anionic dyes, Chemosphere 306 (2022) 135566. https://doi.org/10.1016/j.chemosphere.2022.135566.

[10] G.G. Hacıosmanoğlu, C. Mejías, J. Martín, J.L. Santos, I. Aparicio, E. Alonso, Antibiotic adsorption by natural and modified clay minerals as designer adsorbents for wastewater treatment: A comprehensive review, J. Environ. Manage. 317 (2022) 115397. https://doi.org/10.1016/j.jenvman.2022.115397.

[11] Q. Miao, L. Jiang, J. Yang, T. Hu, S. Shan, H. Su, F. Wu, MOF/hydrogel composite-based adsorbents for water treatment: A review, J. Water Process Eng. 50 (2022) 103348. https://doi.org/10.1016/j.jwpe.2022.103348.

[12] C. Du, Z. Zhang, G. Yu, H. Wu, H. Chen, L. Zhou, Y. Zhang, Y. Su, S. Tan, L. Yang, J. Song, S. Wang, A review of metal organic framework (MOFs)-based materials for antibiotics removal via adsorption and photocatalysis, Chemosphere. 272 (2021) 129501. https://doi.org/10.1016/j.chemosphere.2020.129501.

[13] N. Li, L. Zhou, X. Jin, G. Owens, Z. Chen, Simultaneous removal of tetracycline and oxytetracycline antibiotics from wastewater using a ZIF-8 metal organic-framework, J. Hazard. Mater. 366 (2019) 563–572. https://doi.org/10.1016/j.jhazmat.2018.12.047.

[14] L. Tian, S. Zhou, J. Zhao, Q. Xu, N. Li, D. Chen, H. Li, J. He, J. Lu, Sulfonate-modified calixarene-based porous organic polymers for electrostatic enhancement and efficient rapid removal of cationic dyes in water, J. Hazard. Mater. 441 (2023) 129873. https://doi.org/10.1016/j.jhazmat.2022.129873.

[15] A. Giri, S. Biswas, M.W. Hussain, T.K. Dutta, A. Patra, Nanostructured Hypercrosslinked Porous Organic Polymers: Morphological Evolution and Rapid Separation of Polar Organic Micropollutants, ACS Appl. Mater. Interfaces. 14 (2022) 7369–7381. https://doi.org/10.1021/acsami.1c24393.

[16] D. Luo, M. Li, Q. Ma, G. Wen, H. Dou, B. Ren, Y. Liu, X. Wang, L. Shui, Z. Chen, Porous organic polymers for Li-chemistry-based batteries: functionalities and characterization studies, Chem. Soc. Rev. 51 (2022) 2917–2938. https://doi.org/10.1039/D1CS01014J.

[17] B. Li, R. Gong, W. Wang, X. Huang, W. Zhang, H. Li, C. Hu, B. Tan, A new strategy to microporous polymers: Knitting rigid aromatic building blocks by external cross-linker, Macromolecules. 44 (2011) 2410–2414. https://doi.org/10.1021/ma200630s.

[18] C. Liu, L. Shi, J. Zhang, J. Sun, One-pot synthesis of pyridine-based ionic hyper-cross-linked polymers with hierarchical pores for efficient CO_2 capture and catalytic conversion, Chem. Eng. J. 427 (2022) 131633. https://doi.org/10.1016/j.cej.2021.131633.

[19] Y. Sang, Z. Shu, Y. Wang, L. Wang, D. Zhang, Q. Xiao, F. Zhou, J. Huang, Bifunctional ionic hyper-cross-linked polymers for CO_2 capture and catalytic conversion, Appl. Surf.

Sci. 585 (2022) 152663. https://doi.org/10.1016/j.apsusc.2022.152663.

[20] H. Zhou, C. Rayer, A.R. Antonangelo, N. Hawkins, M. Carta, Adjustable functionalization of hyper-cross-linked polymers of intrinsic microporosity for enhanced CO_2 adsorption and selectivity over N_2 and CH_4, ACS Appl. Mater. Interfaces. 14 (2022) 20997–21006. https://doi.org/10.1021/acsami.2c02604.

[21] S. Hou, J. Hu, X. Liang, D. Zhang, B. Tan, Carbonate-based hyper-cross-linked polymers with pendant versatile electron-withdrawing functional groups for CO_2 adsorption and separation, J. Mater. Chem. A. 10 (2022) 15062–15073. https://doi.org/10.1039/D2TA02774G.

[22] A. Hassan, R. Bera, A. Alam, N. Das, Triptycene based fluorinated polymers with improved carbon dioxide capture and hydrogen/methane storage, Microporous Mesoporous Mater. 346 (2022) 112320. https://doi.org/10.1016/j.micromeso.2022.112320.

[23] A.E. Sadak, E. Cucu, B. Hamur, İ. Ün, R. Altundas, Cyclotriphosphazene and tricarbazole based microporous hyper-crosslinked conjugated polymer for CCUS: Exceptional CO_2 selectivity and high capacity CO_2, CH_4, and H_2 capture, J. CO2 Util. 67 (2023) 102304. https://doi.org/10.1016/j.jcou.2022.102304.

[24] J. Gu, P. Shao, L. Luo, Y. Wang, T. Zhao, C. Yang, P. Chen, F. Liu, Microporous triazine-based ionic hyper-crosslinked polymers for efficient and selective separation of $H_2S/CH_4/N_2$, Sep. Purif. Technol. 285 (2022) 120377. https://doi.org/10.1016/j.seppur.2021.120377.

[25] J. Yan, Y. Tan, L. Wei, Z. Liu, Q. Wang, H. Sun, Z. Wang, D. Li, Y. Qian, S. Guo, Friedel–Crafts synthesis of carbazole-based hierarchical nanoporous organic polymers for adsorption of ethane, carbon dioxide, and methane, Ind. Eng. Chem. Res. 61 (2022) 13453–13460. https://doi.org/10.1021/acs.iecr.2c01931.

[26] A. Waheed, N. Baig, N. Ullah, W. Falath, Removal of hazardous dyes, toxic metal ions and organic pollutants from wastewater by using porous hyper-cross-linked polymeric materials: A review of recent advances, J. Environ. Manage. 287 (2021) 112360. https://doi.org/10.1016/j.jenvman.2021.112360.

[27] G. Paul, F. Begni, A. Melicchio, G. Golemme, C. Bisio, D. Marchi, M. Cossi, L. Marchese, G. Gatti, Hyper-Cross-Linked Polymers for the Capture of Aromatic Volatile

Compounds, ACS Appl. Polym. Mater. 2 (2020) 647–658. https://doi.org/10.1021/acsapm.9b01000.

[28] W.Q. Wang, J. Wang, J.G. Chen, X.S. Fan, Z.T. Liu, Z.W. Liu, J. Jiang, Z. Hao, Synthesis of novel hyper-cross-linked polymers as adsorbent for removing organic pollutants from humid streams, Chem. Eng. J. 281 (2015) 34–41. https://doi.org/10.1016/j.cej.2015.06.095.

[29] H. Ramezanipour Penchah, A. Ghaemi, H. Ganadzadeh Gilani, Benzene-based hyper-cross-linked polymer with enhanced adsorption capacity for CO_2 capture, Energy & Fuels 33 (2019) 12578–12586. https://doi.org/10.1021/acs.energyfuels.9b03136.

[30] X. Luo, J. Shi, H. Zhao, C. Ma, D. Hu, H. Zhang, Q. Shen, N. Sun, W. Wei, Biased adsorption of ethane over ethylene on low-cost hyper-crosslinked polymers, J. Solid State Chem. 271 (2019) 199–205. https://doi.org/10.1016/j.jssc.2018.12.061.

[31] M. Errahali, G. Gatti, L. Tei, G. Paul, G.A. Rolla, L. Canti, A. Fraccarollo, M. Cossi, A. Comotti, P. Sozzani, L. Marchese, Microporous hyper-cross-linked aromatic polymers designed for methane and carbon dioxide adsorption, J. Phys. Chem. C. 118 (2014) 28699–28710. https://doi.org/10.1021/jp5096695.

[32] A.M. James, S. Harding, T. Robshaw, N. Bramall, M.D. Ogden, R. Dawson, Selective Environmental Remediation of Strontium and Cesium Using Sulfonated Hyper-Cross-Linked Polymers (SHCPs), ACS Appl. Mater. Interfaces 11 (2019) 22464–22473. https://doi.org/10.1021/acsami.9b06295.

[33] H.X. Li, X. Zhang, Q. Wang, K. Zhang, Q. Cao, L. Jin, Preparation of the recycled and regenerated mesocarbon microbeads-based solid acid and its catalytic behaviors for hydrolysis of cellulose, Bioresour. Technol. 270 (2018) 166–171. https://doi.org/10.1016/j.biortech.2018.09.037.

[34] E.D. Revellame, D.L. Fortela, W. Sharp, R. Hernandez, M.E. Zappi, Adsorption kinetic modeling using pseudo-first order and pseudo-second order rate laws: A review, Clean. Eng. Technol. 1 (2020) 100032. https://doi.org/10.1016/j.clet.2020.100032.

[35] F.C. Wu, R.L. Tseng, R.S. Juang, Initial behavior of intraparticle diffusion model used in the description of adsorption kinetics, Chem. Eng. J. 153 (2009) 1–8. https://doi.org/10.1016/j.cej.2009.04.042.

[36] D. Lu, S. Xu, W. Qiu, Y. Sun, X. Liu, J. Yang, J. Ma, Adsorption and desorption behaviors of antibiotic ciprofloxacin on functionalized spherical MCM-41 for water treatment, J. Clean. Prod. 264 (2020) 121644. https://doi.org/10.1016/j.jclepro.2020.121644.

[37] S.K. Milonjić, A consideration of the correct calculation of thermodynamic parameters of adsorption, J. Serb. Chem. Soc. 72 (2007) 1363–1367. https://doi.org/10.2298/JSC0712363M.

[38] C.A. Igwegbe, S.N. Oba, C.O. Aniagor, A.G. Adeniyi, J.O. Ighalo, Adsorption of ciprofloxacin from water: A comprehensive review, J. Ind. Eng. Chem. 93 (2021) 57–77. https://doi.org/10.1016/j.jiec.2020.09.023.

[39] P. Puthiaraj, Y.-R. Lee, W.-S. Ahn, Microporous amine-functionalized aromatic polymers and their carbonized products for CO_2 adsorption, Chem. Eng. J. 319 (2017) 65–74. https://doi.org/10.1016/j.cej.2017.03.001.

[40] R.T. Woodward, L.A. Stevens, R. Dawson, M. Vijayaraghavan, T. Hasell, I.P. Silverwood, A. V. Ewing, T. Ratvijitvech, J.D. Exley, S.Y. Chong, F. Blanc, D.J. Adams, S.G. Kazarian, C.E. Snape, T.C. Drage, A.I. Cooper, Swellable, water- and acid-tolerant polymer sponges for chemoselective carbon dioxide capture, J. Am. Chem. Soc. 136 (2014) 9028–9035. https://doi.org/10.1021/ja5031968.

[41] L. Tan, B. Li, X. Yang, W. Wang, B. Tan, Knitting hypercrosslinked conjugated microporous polymers with external crosslinker, Polymer 70 (2015) 336–342. https://doi.org/10.1016/j.polymer.2015.06.026.

[42] J. Byun, S.H. Je, H.A. Patel, A. Coskun, C.T. Yavuz, Nanoporous covalent organic polymers incorporating Tröger's base functionalities for enhanced CO_2 capture, J. Mater. Chem. A. 2 (2014) 12507–12512. https://doi.org/10.1039/c4ta00698d.

[43] S.G. Akpe, I. Ahmed, P. Puthiaraj, K. Yu, W.S. Ahn, Microporous organic polymers for efficient removal of sulfamethoxazole from aqueous solutions, Microporous Mesoporous Mater. 296 (2020) 109979. https://doi.org/10.1016/j.micromeso.2019.109979.

[44] R.M.N. Kalla, M.-R. Kim, I. Kim, Sulfonic Acid-Functionalized, Hyper-Cross-Linked Porous Polyphenols as Recyclable Solid Acid Catalysts for Esterification and Transesterification Reactions, Ind. Eng. Chem. Res. 57 (2018) 11583–11591.

https://doi.org/10.1021/acs.iecr.8b02418.

[45] C. Zhang, Q. Zhuang, H. Wang, X. Ying, R. Ji, D. Sheng, W. Dong, A. Xie, Constructing an acidic microenvironment by sulfonated polymers for photocatalytic reduction of hexavalent chromium under neutral conditions, J. Colloid Interface Sci. 630 (2023) 235–248. https://doi.org/10.1016/j.jcis.2022.10.055.

[46] P.A. Russo, M.M. Antunes, P. Neves, P. V. Wiper, E. Fazio, F. Neri, F. Barreca, L. Mafra, M. Pillinger, N. Pinna, A.A. Valente, Solid acids with SO_3H groups and tunable surface properties: Versatile catalysts for biomass conversion, J. Mater. Chem. A. 2 (2014) 11813–11824. https://doi.org/10.1039/c4ta02320j.

[47] J. Zhang, K. Dong, W. Luo, H. Guan, Catalytic upgrading of carbohydrates into 5-ethoxymethylfurfural using SO_3H functionalized hyper-cross-linked polymer based carbonaceous materials, Fuel. 234 (2018) 664–673. https://doi.org/10.1016/j.fuel.2018.07.060.

[48] C. Pirez, J.M. Caderon, J.P. Dacquin, A.F. Lee, K. Wilson, Tunable KIT-6 mesoporous sulfonic acid catalysts for fatty acid esterification, ACS Catal. 2 (2012) 1607–1614. https://doi.org/10.1021/cs300161a.

[49] M.M. Aboelhassan, A.F. Peixoto, C. Freire, Sulfonic acid functionalized silica nanoparticles as catalysts for the esterification of linoleic acid, New J. Chem. 41 (2017) 3595–3605. https://doi.org/10.1039/c6nj04043h.

[50] L. Zhang, L. Yao, L. Ye, B. Long, Y. Dai, Y. Ding, Benzimidazole-based hyper-cross-linked polymers for effective adsorption of chlortetracycline from aqueous solution, J. Environ. Chem. Eng. 8 (2020) 104562. https://doi.org/10.1016/j.jece.2020.104562.

[51] S. Song, J. Ai, A. Hu, G. Liao, D. Wang, Synthesis of carboxyl-modified hyper-cross-linked polymers with conspicuous removal capability for various water-soluble contaminants, J. Environ. Chem. Eng. 9 (2021) 106047. https://doi.org/10.1016/j.jece.2021.106047.

[52] M. Thommes, K. Kaneko, A. V. Neimark, J.P. Olivier, F. Rodriguez-Reinoso, J. Rouquerol, K.S.W. Sing, Physisorption of gases, with special reference to the evaluation of surface area and pore size distribution (IUPAC Technical Report), Pure Appl. Chem. 87 (2015) 1051–1069. https://doi.org/10.1515/pac-2014-1117.

[53] S. Bhunia, B. Banerjee, A. Bhaumik, A new hypercrosslinked supermicroporous polymer, with scope for sulfonation, and its catalytic potential for the efficient synthesis of biodiesel at room temperature, Chem. Commun. 51 (2015) 5020–5023. https://doi.org/10.1039/c4cc09872b.

[54] S.K. Kundu, A. Bhaumik, Pyrene-Based Porous Organic Polymers as Efficient Catalytic Support for the Synthesis of Biodiesels at Room Temperature, ACS Sustain. Chem. Eng. 3 (2015) 1715–1723. https://doi.org/10.1021/acssuschemeng.5b00238.

[55] L. Sekerová, P. Březinová, T.T. Do, E. Vyskočilová, J. Krupka, L. Červený, L. Havelková, B. Bashta, J. Sedláček, Sulfonated Hyper-cross-linked Porous Polyacetylene Networks as Versatile Heterogeneous Acid Catalysts, ChemCatChem 12 (2020) 1075–1084. https://doi.org/10.1002/cctc.201901815.

[56] Y. Cheng, S. Razzaque, Z. Zhan, B. Tan, Construction and gas uptake performance of cyano-functional hypercrosslinked polymers via knitting strategy, Chem. Eng. J. 426 (2021). https://doi.org/10.1016/j.cej.2021.130731.

[57] J. Wolska, K. Stawicka, J. Walkowiak-Kulikowska, Sulfonic-acid-functionalized polymers based on fluorinated methylstyrenes and styrene as promising heterogeneous catalysts for esterification, Mater. Chem. Phys. 273 (2021) 125132. https://doi.org/10.1016/j.matchemphys.2021.125132.

[58] S. Jiang, Z. Li, X. Yang, M. Li, C. Wang, Z. Wang, Q. Wu, Sustainable and green synthesis of porous organic polymer for solid-phase extraction of four chlorophenols in water and honey, Food Chem. 404 (2023) 134652. https://doi.org/10.1016/j.foodchem.2022.134652.

[59] Z. Zhu, J. Xie, M. Zhang, Q. Zhou, F. Liu, Insight into the adsorption of PPCPs by porous adsorbents: Effect of the properties of adsorbents and adsorbates, Environ. Pollut. 214 (2016) 524–531. https://doi.org/10.1016/j.envpol.2016.04.070.

[60] R. Allgayer, N. Yousefi, N. Tufenkji, Graphene oxide sponge as adsorbent for organic contaminants: comparison with granular activated carbon and influence of water chemistry, Environ. Sci. Nano. 7 (2020) 2669–2680. https://doi.org/10.1039/d0en00193g.

[61] J. Cheng, J.J. Gu, W. Tao, P. Wang, L. Liu, C.Y. Wang, Y.K. Li, X.H. Feng, G.H. Qiu, F.F. Cao, Edible fungus slag derived nitrogen-doped hierarchical porous carbon as a

high-performance adsorbent for rapid removal of organic pollutants from water, Bioresour. Technol. 294 (2019) 122149. https://doi.org/10.1016/j.biortech.2019.122149.

[62] V.C. Ramos, W. Han, K.L. Yeung, Functionalization of metal organic frameworks by [BMIM][CH_3COO] ionic liquid for toluene capture, Environ. Res. 215 (2022) 114341. https://doi.org/10.1016/j.envres.2022.114341.

[63] Y. Ho, G. McKay, Pseudo-second order model for sorption processes, Process Biochem. 34 (1999) 451–465. https://doi.org/10.1016/S0032-9592(98)00112-5.

[64] G. Guzel Kaya, E. Aznar, H. Deveci, R. Martínez-Máñez, Low-cost silica xerogels as potential adsorbents for ciprofloxacin removal, Sustain. Chem. Pharm. 22 (2021) 100483. https://doi.org/10.1016/j.scp.2021.100483.

[65] S. Ravi, Y. Choi, J.K. Choe, Novel phenyl-phosphate-based porous organic polymers for removal of pharmaceutical contaminants in water, Chem. Eng. J. 379 (2020) 122290. https://doi.org/10.1016/j.cej.2019.122290.

[66] R. Antonelli, G.R.P. Malpass, M.G.C. Da Silva, M.G.A. Vieira, Adsorption of ciprofloxacin onto thermally modified bentonite clay: Experimental design, characterization, and adsorbent regeneration, J. Environ. Chem. Eng. 8 (2020) 104553. https://doi.org/10.1016/j.jece.2020.104553.

[67] R. Kumar, J. Rashid, M.A. Barakat, Synthesis and characterization of a starch-AlOOH-FeS_2 nanocomposite for the adsorption of congo red dye from aqueous solution, RSC Adv. 4 (2014) 38334–38340. https://doi.org/10.1039/c4ra05183a.

[68] M. Yilimulati, L. Wang, X. Ma, C. Yang, N. Habibul, Adsorption of ciprofloxacin to functionalized nano-sized polystyrene plastic: Kinetics, thermochemistry and toxicity, Sci. Total Environ. 750 (2021) 142370. https://doi.org/10.1016/j.scitotenv.2020.142370.

[69] S. Raghav, D. Kumar, Adsorption Equilibrium, Kinetics, and Thermodynamic Studies of Fluoride Adsorbed by Tetrametallic Oxide Adsorbent, J. Chem. Eng. Data. 63 (2018) 1682–1697. https://doi.org/10.1021/acs.jced.8b00024.

[70] A.A. Aryee, F.M. Mpatani, A.N. Kani, E. Dovi, R. Han, Z. Li, L. Qu, Iminodiacetic acid functionalized magnetic peanut husk for the removal of methylene blue from solution: characterization and equilibrium studies, Environ. Sci. Pollut. Res. 27 (2020) 40316–40330. https://doi.org/10.1007/s11356-020-10087-6.

[71] S. Mortazavian, A. Saber, J. Hong, J.H. Bae, D. Chun, N. Wong, D. Gerrity, J. Batista, K.J. Kim, J. Moon, Synthesis, characterization, and kinetic study of activated carbon modified by polysulfide rubber coating for aqueous hexavalent chromium removal, J. Ind. Eng. Chem. 69 (2019) 196–210. https://doi.org/10.1016/j.jiec.2018.09.028.

[72] J. Gu, J. Zhang, D. Li, H. Yuan, Y. Chen, Hyper-cross-linked polymer based carbonaceous materials as efficient catalysts for ethyl levulinate production from carbohydrates, J. Chem. Technol. Biotechnol. 94 (2019) 3073–3083. https://doi.org/10.1002/jctb.6107.

[73] A.A. Raza, S. Ravi, S.S. Tajudeen, A.K.I. Sheriff, Trifunctional covalent triazine and carbonyl based polymer as a catalyst for one-pot multistep organic transformation, React. Funct. Polym. 167 (2021) 105011. https://doi.org/10.1016/j.reactfunctpolym.2021.105011.

[74] A. Munyentwali, C. Li, H. Li, Q. Yang, Synthesis of Sulfonated Porous Organic Polymers with a Hydrophobic Core for Efficient Acidic Catalysis in Organic Transformations, Chem. - An Asian J. 16 (2021) 2041–2047. https://doi.org/10.1002/asia.202100456.

[75] M. Nazraz, Y. Yamini, H. Asiabi, Chitosan-based sorbent for efficient removal and extraction of ciprofloxacin and norfloxacin from aqueous solutions, Microchim. Acta. 186 (2019) 459. https://doi.org/10.1007/s00604-019-3563-x.

[76] M.Z. Afzal, X.F. Sun, J. Liu, C. Song, S.G. Wang, A. Javed, Enhancement of ciprofloxacin sorption on chitosan/biochar hydrogel beads, Sci. Total Environ. 639 (2018) 560–569. https://doi.org/10.1016/j.scitotenv.2018.05.129.

[77] A.A. Mohammed, T.J. Al-Musawi, S.L. Kareem, M. Zarrabi, A.M. Al-Ma'abreh, Simultaneous adsorption of tetracycline, amoxicillin, and ciprofloxacin by pistachio shell powder coated with zinc oxide nanoparticles, Arab. J. Chem. 13 (2020) 4629–4643. https://doi.org/10.1016/j.arabjc.2019.10.010.

[78] Q. Yang, H. Yu, Y. He, Z. Liu, C. Qin, B. Liu, Y. Li, Porous three-component hybrid hydrogen-bonded covalent organic polymers: Design, synthesis and ciprofloxacin adsorption, Eur. Polym. J. 123 (2020) 109445. https://doi.org/10.1016/j.eurpolymj.2019.109445.

[79] J. Ma, M. Yang, F. Yu, J. Zheng, Water-enhanced Removal of Ciprofloxacin from Water

by Porous Graphene Hydrogel, Sci. Rep. 5 (2015) 1–10. https://doi.org/10.1038/srep13578.

[80] Z. Wang, Y. Muhammad, R. Tang, C. Lu, S. Yu, R. Song, Z. Tong, B. Han, H. Zhang, Dually organic modified bentonite with enhanced adsorption and desorption of tetracycline and ciprofloxacin, Sep. Purif. Technol. 274 (2021) 119059. https://doi.org/10.1016/j.seppur.2021.119059.

[81] M.M.M. Ali, M.J. Ahmed, B.H. Hameed, NaY zeolite from wheat (Triticum aestivum L.) straw ash used for the adsorption of tetracycline, J. Clean. Prod. 172 (2018) 602–608. https://doi.org/10.1016/j.jclepro.2017.10.180.

[82] B.K. Vu, O. Snisarenko, H.S. Lee, E.W. Shin, Adsorption of tetracycline on La-impregnated MCM-41 materials, Environ. Technol. 31 (2010) 233–241. https://doi.org/10.1080/09593330903453210.

[83] A. Hu, L. Liqing, M. Zhang, Y. Liu, G. Liao, D. Wang, Synthesis of highly water-dispersible adsorbent derived from alkali-modified hyper-cross-linked polymer for efficient removal of various organic contaminants and ammonia, J. Water Process Eng. 40 (2021) 101902. https://doi.org/10.1016/j.jwpe.2020.101902.

[84] J. Imanipoor, A. Ghafelebashi, M. Mohammadi, M. Dinari, M.R. Ehsani, Fast and effective adsorption of amoxicillin from aqueous solutions by L-methionine modified montmorillonite K10, Colloids Surfaces A Physicochem. Eng. Asp. 611 (2021) 125792. https://doi.org/10.1016/j.colsurfa.2020.125792.

[85] J. Imanipoor, M. Mohammadi, M. Dinari, M.R. Ehsani, Adsorption and Desorption of Amoxicillin Antibiotic from Water Matrices Using an Effective and Recyclable MIL-53(Al) Metal-Organic Framework Adsorbent, J. Chem. Eng. Data. 66 (2021) 389–403. https://doi.org/10.1021/acs.jced.0c00736.

[86] M.N. Alnajrani, O.A. Alsager, Removal of Antibiotics from Water by Polymer of Intrinsic Microporosity: Isotherms, Kinetics, Thermodynamics, and Adsorption Mechanism, Sci. Rep. 10 (2020) 1–14. https://doi.org/10.1038/s41598-020-57616-4.

[87] H. Kim, S. Yang, D.H. Kim, One-pot conversion of alginic acid into furfural using Amberlyst-15 as a solid acid catalyst in γ-butyrolactone/water co-solvent system, Environ. Res. 187 (2020) 109667. https://doi.org/10.1016/j.envres.2020.109667.